Novel 3D printed TPMS scaffolds: microstructure, characteristics and applications in bone regeneration

Jiaqi Ma[1][†] [iD], Yumeng Li[1][†], Yujing Mi[2], Qiannan Gong[3], Pengfei Zhang[4], Bing Meng[1], Jue Wang[5], Jing Wang[6] and Yawei Fan[1]

Abstract
Bone defect disease seriously endangers human health and affects beauty and function. In the past five years, the three dimension (3D) printed radially graded triply periodic minimal surface (TPMS) porous scaffold has become a new solution for repairing bone defects. This review discusses 3D printing technologies and applications for TPMS scaffolds. To this end, the microstructural effects of 3D printed TPMS scaffolds on bone regeneration were reviewed and the structural characteristics of TPMS, which can promote bone regeneration, were introduced. Finally, the challenges and prospects of using TPMS scaffolds to treat bone defects were presented. This review is expected to stimulate the interest of bone tissue engineers in radially graded TPMS scaffolds and provide a reliable solution for the clinical treatment of personalised bone defects.

[1]Department of Oral and Maxillofacial Surgery, First Hospital of Shanxi Medical University, Taiyuan, China
[2]Department of Orthodontics, First Hospital of Shanxi Medical University, Taiyuan, China
[3]Shanxi Provincial People's Hospital of Stomatology,Taiyuan,China
[4]Shanxi Medical University School and Hospital of Stomatology, Taiyuan, China
[5]Department of Prosthodontics, First Hospital of Shanxi Medical University, Taiyuan, China
[6]State Key Laboratory of Oral & Maxillofacial Reconstruction and Regeneration, National Clinical Research Center for Oral Diseases, Shaanxi Engineering Research Center for Dental Materials and Advanced Manufacture, Department of Oral Implants, School of Stomatology, The Fourth Military Medical University, Xi'an, People's Republic of China

[†]These authors contributed equally to this work.

Corresponding authors:
Jing Wang, State Key Laboratory of Oral & Maxillofacial Reconstruction and Regeneration, National Clinical Research Center for Oral Diseases, Shaanxi Engineering Research Center for Dental Materials and Advanced Manufacture, Department of Oral Implants, School of Stomatology, The Fourth Military Medical University, Changle West Road 145#, Xi'an 710032, China.
Email: wangjfmmu@163.com

Yawei Fan, Department of Oral and Maxillofacial Surgery, First Hospital of Shanxi Medical University, Xinjian South Road 85#, Taiyuan 030001, China.
Email: yaweifan1970@163.com

Introduction

Bone defect disease is commonly caused by congenital defects, trauma, degenerative diseases, tumours and infection necrosis (osteomyelitis), has become a global health problem of great concern.[1,2] Bone defects beyond the critical range cannot heal naturally, and the currently recognised critical size defect for humans is a defect length greater than 1–2 cm and a loss of bone circumference greater than 50%.[3] A traditional clinical treatment strategy is promoting bone regeneration and reconstructing the defect by implanting bone graft materials (autologous bone, allogeneic bone and xenograft bone).[4,5] However, there are drawbacks to these bone transplants, which includes significant surgical stress, poor bone supply, disease transmission risk and loss of three dimension (3D) perception.[5] Bone tissue engineering offers a solution to these defects.

The human bone tissue is an uneven scaffold with internal porosity between 50% and 90%, and different bones have different porosity and structure.[6] Consequently, the design of a 3D printed porous scaffold is required, particularly of a gradient scaffold with radial grading pores and pore diameters that can be parameterised in accordance with the unique properties of each bone tissue.[6] Triply periodic minimal surfaces (TPMS) are infinite, non-self-intersecting 3D periodic surface structures,[7] and in mathematics, TPMS is referred to as a surface with infinite duplication in three dimensions and zero mean curvature.[8] A TPMS scaffold is a new type of radial hierarchical porous scaffold that has become a research hotspot in the recent five years. However, the ability of TPMS scaffolds to promote bone regeneration remains unclear. The TPMS scaffold can match the characteristics of the surrounding bone tissue and provide an ideal growth environment for osteoblast growth, thereby enabling cells to survive and distribute evenly for replacing defective bones.[9–11] Some scholars proved that 3D printed TPMS scaffolds implanted in animals show good inward bone growth, and a stable interface is formed between the scaffolds and surrounding bone tissue.[12–14]

With the development of tissue engineering, scholars found that radially graded TPMS scaffolds are more suitable for personalised bone defects, and smooth transitions within the scaffolds have become key. The pore size of a TPMS is influenced by the cell size and horizontal parameters, both of which can be controlled effectively by adjusting the parameters in the mathematical equation while maintaining a smooth transition.[15] In 2011, Yoo proposed a hybrid method of distance field and TPMS for perfectly preserving the interconnected pore network in each subscaffold.[16] Similarly, it is easy to merge multiple subscaffolds without any of the sharp features commonly found in the results of Boolean union operations using the mathematical definition and implicit modelling methods of TPMS.[11] Later, these methods were placed into practice, and the scholars successfully prepared radially graded TPMS scaffolds. Thus far, scholars have investigated a hybrid PLA scaffold that combines the lattice structure of the different types of TPMS with a combination of different morphologies and porosity levels that can simulate the transition between the trabecular and cortical bones, thereby replacing damaged areas at the tissue interface.[17]

Although there are many excellent reviews that describe mathematical modelling, structure and advantages and disadvantages of TPMS, few have provided a comprehensive and systematic summary of TPMS.[18–20]

In this review, we summarise the history of 3D printing techniques for TPMS scaffolds and the use of TPMS structures for 3D printing scaffolds. The effects of the microstructure of TPMS on bone regeneration and structural characteristics of TPMS are introduced, and the advantages of TPMS in promoting bone regeneration are emphasised. This review aims to enable more researchers to understand the TPMS scaffold and provide a new choice for the clinical repair of personalised bone defects. The radially graded TPMS scaffold can be used to treat maxillofacial bone defects.

3D printing technology in the TPMS scaffold

3D printing technology is required to make the TPMS scaffold a reality. Further, additive manufacturing, also referred to as 3D printing technology, can produce very detailed models with minimal time and resource loss.[21] Three dimension printing technologies include fused deposition modelling (FDM), lithographic-based, extrusion-based and 3D bioprinting methods.[22] This section provides a quick overview of the 3D printing technologies utilised in TPMS scaffolds as well as a summary of their uses in the scaffolds.

Currently, only four 3D printing technologies are used for fabricating TPMS scaffolds: FDM, lithography-based 3D printing, extrusion-based 3D printing and selective laser melting (SLM). Garcia et al.[23] prepared a TPMS-structured polycaprolactone scaffold using extrudation-based 3D printing technology, which can be used as a replacement for bone defects. Stereolithography (SLA), digital light processing (DLP) and other lithography-based 3D printing techniques can be categorised. Yang subcutaneously inserted SLA-printed β-tricalcium phosphate (β-TCP) TPMS scaffolds into male C57 mice.[24] The TPMS group outperformed the cross scaffolds in terms of the inward development of new tissue, and after 35 days, it exhibited greater integration with the surrounding host tissue that that with the cross scaffolds.[24] DLP uses a digital light projector instead of the mirrors used in SLA for reflecting the laser source.[25] Bouakaz et al.[26] used DLP to print a TPMS hydtoxyapatite (HA) scaffold with a 900 μm

pore size, 72% theoretical porosity and 200 µm wall thickness. They employed a big animal model, sheep, in vivo and Bio-Oss R© as a control, in contrast to that used in earlier research. Owing to its superior bone conduction capabilities and osseous integration capability, Bio-Oss R© has been the go-to reference in stomatology and utilised as a standard in orthopaedics for many years. The scaffold outperformed Bio-Oss R© in terms of early healing (in terms of bone integration and homologous mineralisation), showed good bone regeneration and they had the same high permeability as natural trabecular bone based on their thorough analyses conducted over both short term (4 weeks) and long term (26 weeks).[26] The application of 3D printing technology in the TPMS scaffold is summarised in Table 1.

Microstructure of the TPMS scaffold

Cortical and cancellous bones combine to form complex natural bone structures. The cancellous bone offers room for blood vessels and bone marrow penetration as well as strong connections for metabolic activity.[42] The cortical bone is far denser than the cancellous bone and serves as a support, shielding the latter and serving as a lever for movement.[9] A TPMS scaffold is a bionic scaffold whose microstructure is similar to that of the bone and affects bone conduction. The process by which progenitor cells, perivascular tissue and germinated capillaries grow inward from the bone bed to the 3D structure of the porous scaffold – which acts as a guiding cue for bridging the bone – is known as bone conduction.[43] In bone tissue engineering, bone conduction is dependent on a scaffold microstructure.[43] In bone conduction, which is inextricably linked to its microstructure, TPMS offers significant advantages, in that the geometry, wall thickness, pore size, porosity and surface curvature of the TPMS scaffold comprises its microstructure.

Geometry

Pore shape has a significant effect on tissue growth, osteoclast activity and degradation rate in biological scaffolds.[44] Adequate scaffolding in terms of the pore shape can offer sufficient room for cell activity.[45] In a basic reaction-diffusion model, Buenzli et al.[46] demonstrated that pore geometry affects cell density while restricting cell migration and division. In nature, biological tissues that include TPMS structures are beetle shells, weevils, butterfly wing scales and crustacean skeletons.[47] The minimal surface structure in natural organisation follows the concept of free energy minimisation, which is a physical law governing object shape and motion. Organisms frequently attempt to organise themselves to use less energy for better stability in both natural and artificial

contexts.[48] Consequently, items with a TPMS structure are more stable. Owing to the intricate and extremely cubic symmetric structure of TPMS, cubic translational cell periodicity enables its recurrent construction.[47] The TPMS structure is designed by drawing inspiration from nature. When German mathematician Hermann Schwarz released his article on primitive and diamond surfaces in 1865, the TPMS was stated in print for the first time. His pupil Edvard Rudolf Neovius described a surface based on TPMS in 1883, which is now referred to as Neovius.[20] Alan Hugh Schoen published numerous other TPMS-based surfaces, including gyroid, which is among the most well-known TPMS structures to date, exactly 100 years before.[20] A total of 16 TPMS structures – C(Y), C(D), Schwarz D (diamond), Schwarz P (primitive), batwing, F-RD, I-WP, Manta 35, Fischer–Koch S, Fischer–Koch Y, Neovius, split-P, Dprime, lindinoid, isometric wrapped surfaces and gyroid – for 3D printing scaffolds have been referenced in prior research.[7,8,10,36,47,49] A straightforward reaction-diffusion model developed by Buenzli et al. demonston. The shapes of these TPMS structures differ. A straightforward reaction-diffusion model developed by Buenzli et al. demonstrates that the shapes of the TPMS structures differ. A brief timeline of the development of these TPMS structures for 3D-printing scaffolds is shown in Figure 1.[11,50]

Numerous researchers have focussed on these three structures because the gyroid structure mirrors the shape of the bone trabeculae, and the primitive and diamond structures both have significant load-carrying capacities.[11,51] Their structures are shown in Figure 2.[11] The most widely utilised TPMS shape is the gyroid structure, which lacks a reflective symmetric surface and straight segments on its surface. The constant curve helps prevent stress concentration.[52] Studies show that the gyroid scaffold retains good mechanical properties even after six months of biodegradation.[53] The first practical application of TPMS to bone tissue engineering scaffolders was presented in 2006 by Rajagopalan and Robb.[54] Since then, TPMS structures have been used in bone tissue engineering by an increasing number of researchers.

Summary. At present, there are 16 TPMS structures mentioned in the literature for 3D printing scaffolds, and the three most used are gyroids, diamonds and primitives. Each TPMS structure has a different geometry, and we believe that more TPMS structures will emerge for future use in tissue engineering.

Wall thickness

Topological features, or wall thickness, are used to categorise TPMS structures into two groups: sheet structures and skeleton structures.[47] With the use of solid materials,

Table I. Summary of application of 3D printing technology in TPMS scaffold.

| 3D-printing technology	Materials	TPMS structure	In vivo/in vitro	Applications	Reference
FDM	Polyether ether ketone,silicon nitride and	Gyroid	In vitro (Mouse preosteoblast cells)	Spinal implants	Du et al.[27]
	PLA	Diamond, Schwarz and Gyroid	In vitro (Osteoblast-like cells)	Bone implants	Diez-Escudero et al.[28]
	PLA, graphene oxide	Primitive and Gyroid	In vitro (Bone marrow mesenchymal stem cells)	Bone tissue engineering	Guo et al.[29]
Extrusion-based 3D printing technology	Polycaprolactone	Gyroid	In vitro (Physical property test)	Bone regeneration	Garcia et al.[23]
Stereolithography-based	Zn-1Mg	Gyroid	In vitro (Mouse osteoblasts cells)	Repair of bone defects	Chen et al.[30]
	Very Grey Full Cure850, Full Cure750 photopolymer resins	Primitive and Diamond	In vitro (Mechanical compressive test and finite element analysis)	Research mechanical properties and deformation mechanisms of TPMS scaffold	Afshar et al.[31]
	Poly (trimethylene carbonate)	Diamond, Gyroid, Schwarz P, Fischer–Koch S and F-RD	In vitro (Physical property test)	Bone tissue engineering	Blanquer et al.[32]
	HA	Fischer–Koch S	In vitro (Physical property test)	Bone tissue engineering	Baumer et al.[33]
SLA	β-TCP	Gyroid	In vitro (Human mesenchymal stem cells) and In vivo (Rabbit)	Bone regeneration	Yang et al.[24]
	HA	Split-P, Diamond, Primitive, Dprime, Lindinoid and Gyroid	In vitro (Osteoblast) and In vivo(Rabbit)	Bone tissue engineering	Zhang et al.[7]
DLP	HA	Gyroid	In vivo (Sheep)	Bone regeneration	Bouakaz et al.[26]
	Wollastonite powders	Gyroid,Diamond and I-WP	In vitro (Bone marrow mesenchymal stem cells) and In vivo (Rabbit)	Repair of bone defects	Shen et al.[13]
	HA	Gyroid	In vitro (Bone marrow mesenchymal stem cells)	Bone regeneration	Liu et al.[34]
SLM	Ti6Al4V	Fischer–Koch S, Gyroid and Diamond	In vitro (Rat bone marrow mesenchymal stem cells)	Repair of bone defects	Lv et al.[35]
	Ti6Al4V	Gyroid and Diamond	In vitro (Mechanical tests and finite element analysis)	Repair of bone defects	Naghavi et al.[36]
	Ti6Al4V	Primitive,Diamond and I-WP	In vitro (Human osteosarcoma cells)	In vitro evaluation	Myakinin et al[37]
	Ti6Al4V	Gyroid	In vitro (Bone marrow mesenchymal stem cells) and In vivo (Rabbit)	Bone regeneration	Wang et al.[38]
	Ni46.5Ti44.5Nb9 alloy	Gyroid	In vitro (Mechanical tests and finite element analysis)	Repair of bone defects	Lv et al.[39]
	Ti6Al4V	Primitive, Diamond and Gyroid	In vitro (The fibroblast 3T3 cell)	Hip implants	Davoodi et al.[40]
	AlSi10Mg	Primitive and I-WP	In vitro (Mechanical tests and finite element analysis)	Bone tissue engineering	Li et al.[41]
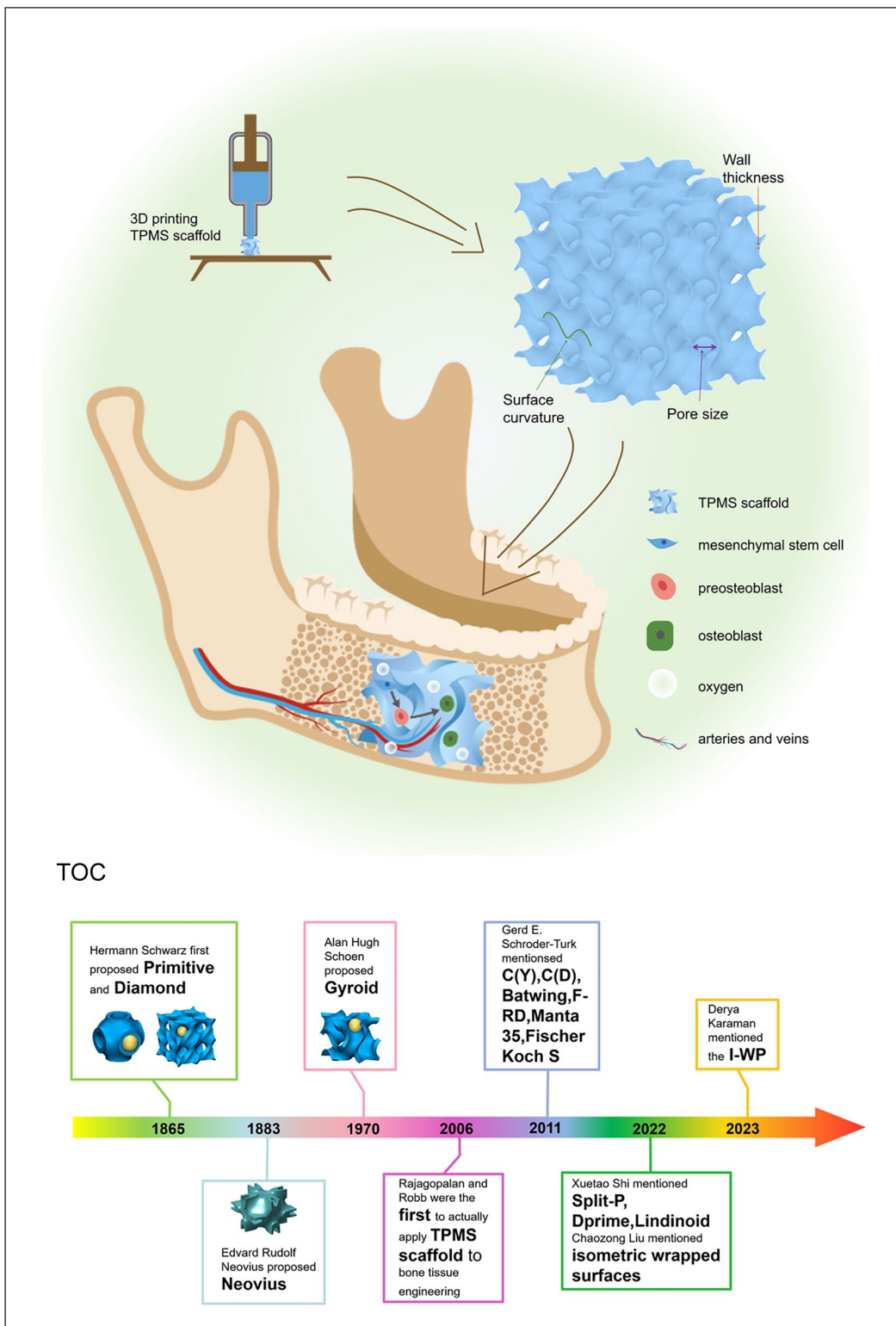
Figure 1. A brief timeline of the development of TPMS structures for 3D-printing scaffolds. 'Primitive', 'Diamond' and 'Gyroid' reproduced from Vijayavenkataraman et al.[11] with permission from Copyright 2018 American Chemical Society. 'Neovius' reproduced from Maskery et al.[50] with permission from Copyright 2021 Springer Nature.
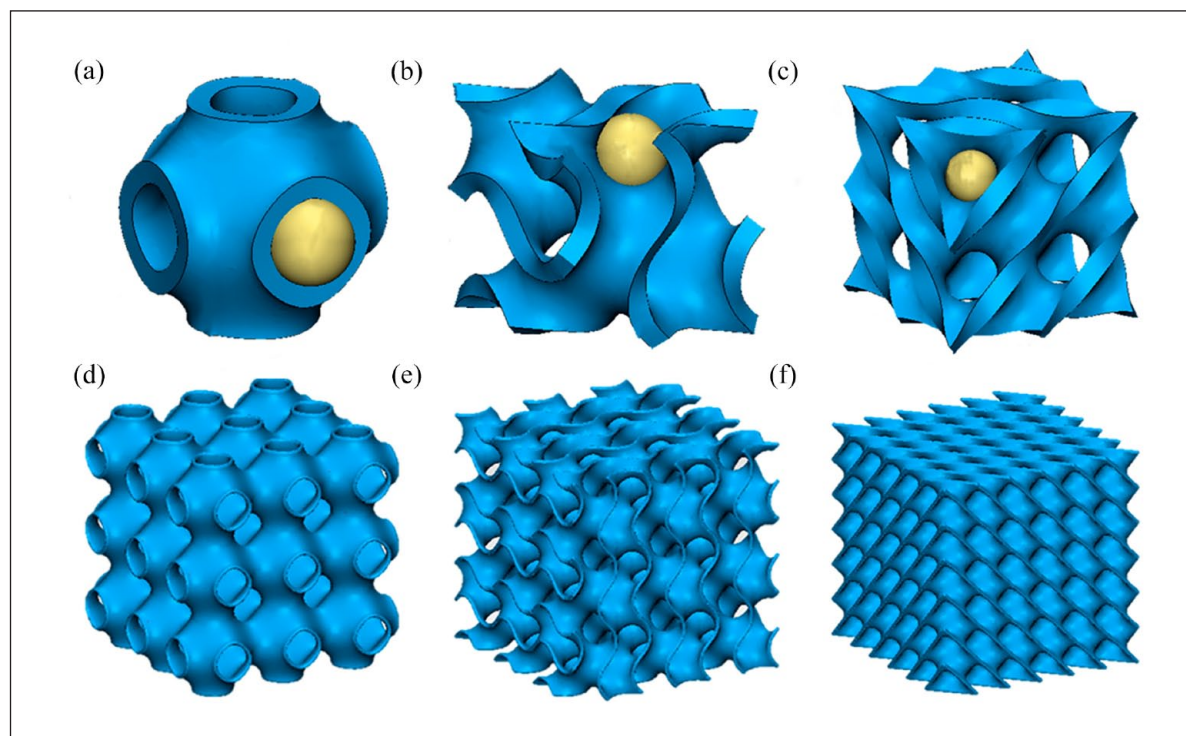
Figure 2. (a–c) The Primitive, gyroid and diamond cell structure respectively. (d–f) Repetitive cell, where pore sizes are marked by yellow. Reproduced from Vijayavenkataraman et al.[11] with permission from Copyright 2018 American Chemical Society.

Vijayavenkataraman et al.[11] thickened and dispersed TPMS to construct thin-walled structures called TPMS sheet scaffolds. Another TPMS-based structure, referred to as the skeleton TPMS structure, is created by adding solid elements to a subspace divided by TPMS.[11] In contrast, TPMS chip scaffolds are mostly utilised for research and have superior mechanical qualities and a larger surface area.[11,15,55] Similarly, according to Al-Ketan et al.'s[56] finite element analysis, sheet lattices have better elastic properties than skeleton lattices. The diamond crystals in the lamellar structure are more fragile and weaker than the gyroid crystals.[57] Shen et al. found that the initial compressive strength of sheet TPMS scaffolds (diamond and gyroid) was three to four times higher than that of bone-like scaffolds, while the bone-like gyroid and diamond scaffolds significantly induced osteogenic differentiation of bone marrow mesenchymal stem cells (BMSC).[13] This result is similar to that reported in Lv et al.'s[35] study. They utilised three structures (Fischer–Koch S, diamond and gyroid) in conjunction with four constants C (0.0, 0.2, 0.4 and 0.6), which represent wall thickness, to 3D print 12 TPMS scaffolds. The higher the C value, the thinner is the wall. The results demonstrated that thick TPMS scaffolds cultivated with rat mesenchymal stem cells (rMSCs) 1, 4 and 7 days later had considerably higher cell viability than that of the thin TPMS scaffolds. This suggests that TPMS scaffolds resembling bones can greatly enhance bone regrowth (Figure 3).[35]

The potential for cell development can be ascertained using fluid dynamics analysis, which is connected to the flow inlet area (m^2) of the scaffold. Karaman et al.[8] discovered that the flow inlet area in the sheet structure is less than that in the skeleton structure in diamond scaffolds with the same porosity. The flow inlet area of sheet structures with the same porosity in gyroid and I-WP scaffolders is greater than that of the skeletal structures.[8] A total of 12 lattice structures, comprising 6 TPMS structures with skeleton and sheet structures, were designed based on the actual allowable design space for TPMS-based lattice selection determined by Gunther et al.[58] based on key parameters and subsequent weighting of them according to additional benefit parameters. The optimal choice for cortical bone was determined to be the Schwarz P lattice, which has a pore size, volume fraction and Young's modulus of 67.572 μm, 0.5445 and 18.758 GPa, respectively. The gyroid bone lattice with a diameter, volume fraction and Young's modulus of 401.39 μm, 0.3 and 4.6835 GPa, respectively, was the most suitable option for the trabecular bone.[58]

Summary. TPMS sheet scaffolds have better mechanical properties and larger surface areas than bone scaffolds, and bone TPMS scaffolds promote bone
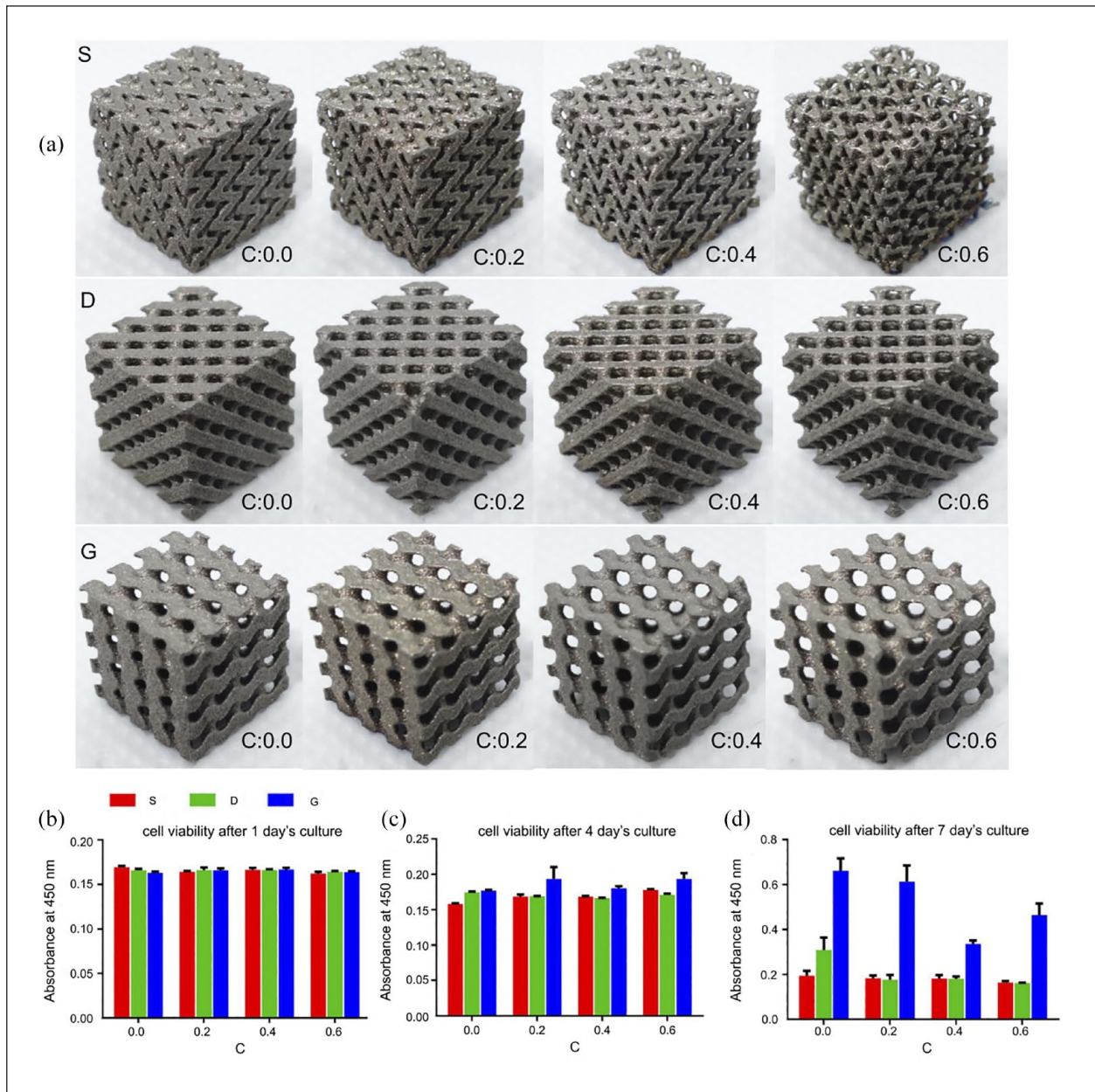
Figure 3. (a) Four different thicknesses of Fischer-Koch S (S), diamond (D) and gyroid (G) scaffolds. The higher the C value, the thinner the wall thickness. (b–d) Comparison of rMSCs proliferation of these scaffolds with different thicknesses at 1,4 and 7 days respectively. Reproduced from Lv et al.[35] with permission from Copyright 2022 Frontiers Media S.A.

regeneration more significantly than sheet scaffolds. Therefore, it is important to select the thickness according to the different experimental requirements and bone defect sites.

Pore size

The 3D printed scaffold must have an open network of pores with an interconnection of more than 100 μm between pores to provide a channel for the vascularised bone to grow inward.[59] The majority of the initial cell attachment occurred in scaffolds with 120 μm pore sizes.[60] Smaller pore scaffolds encourage greater cell attachment initially; however, with longer culture durations, this reverses and they create occlusion, which lowers the permeability of scaffolds.[28,60] Ti6Al4V was utilised by Naghavi et al.[36] to create diamond and gyroid scaffolds with variable cell sizes and a constant wall thickness of 300 μm to create a range of pore diameters. The compressive strength of the cortical bone constructed with both the gyroid (pore size less than 800 μm) and diamond scaffolds (pore size less than 1200 μm), was predicted using

the finite element method along with other mechanical properties such as stiffness and yield strength. When squeezed, the diamond scaffold was ~48% stronger and ~65% stiffer than the gyroid scaffold at the same aperture.[36] The best lattice structure options for bone replacement applications are the gyroid scaffold, which has a diameter of 500–800 μm and porosity of 50$–62% when the sheet thickness is 300 μm, and the diamond scaffold, which has a diameter of 700–1200 μm and porosity of 50%–64.6%.[36] According to certain researchers, the gyroid scaffold with a 792 μm diameter is appropriate for bone regeneration, which is in line with the findings of Naghavi et al.[38] Collagen synthesis is well recognised as a key indicator of osteoblast activity.[37] Cell attachment is mostly dependent on pore size, with a 520 μm pore size scaffold offering more cell attachment sites than the 330 μm pore size scaffold. Research has indicated that, in contrast to TPMS scaffolds measuring 320 μm in diameter, scaffolds measuring 520 μm in diameter sustained cell proliferation from the first to the seventh day of the experiment. In addition, the high rates of collagen formation were noted in both the diamond and I-WP scaffolds measuring 520 μm in diameter.[37] Chen et al.[30] used lithographic-based 3D printing technology to create a Zn-1Mg porous scaffold with a gyroid structure. Bioscaffolds with pore sizes of 650, 800 and 1040 μm were compared for their technical qualities, mechanical properties, corrosion behaviour, biocompatibility and antibacterial capabilities. The study revealed that porous scaffolds with pore sizes of 650 μm exhibited superior mechanical qualities and antibacterial ability, as well as inducing more calcium and phosphorus compounds during the disintegration process.[30] A study on a 3D printed TPMS scaffold with pore sizes ranging from 700 to 1750 μm was conducted by Wang et al.[38] Following four days of cell culture, they discovered that the majority of the cells were dispersed around the surface of the scaffold and that many of the cells were adhered to the wall of the porous scaffold, which had pores that were almost 700 μm in size. The cells on the scaffold with pore sizes of almost 700 μm moved to the adjacent pore after 14 days. Collagen fibrous bone was discovered to be discontinuous in vivo on a scaffold whose pore size was nearly 1750 μm, which was unfavourable to the development of new bone.[38] For a uniform scaffold with a fixed aperture, the permeability increases with the aperture size. The scaffold featuring a radial-gradient aperture exhibited superior permeability and higher mechanical strength than that of the scaffold with a fixed aperture when a fixed porosity was present. Lv et al.[39] conducted experiments wherein they 3D printed gyroid structures with fixed apertures and progressively larger apertures from the inside out. The results indicated that the permeability of the structures with a radial gradient structure and apertures ranging from 500 to 900 μm was similar to that of the structures with apertures of

900 μm.[39] According to Afshar et al.'s[31] study, hierarchical structures are less susceptible to elastic deformation compared with uniform structures.

Summary. A gyroid scaffold with a 600–800 μm pore size is excellent in both mechanical strength and permeability, while the diamond and I-WP scaffolds with a 520 μm pore size are suitable, which can be selected according to different bone defects. However, the TPMS gradient-aperture scaffold was superior to the TPMS uniform-aperture scaffold.

Porosity

A scaffold has the natural porosity of cortical bones, and therefore, a low-porosity scaffold of 10%–30% is needed to replace them, whereas a high-porosity scaffold of 50%–80% is required to repair injured trabecular bones.[17,61] According to certain researchers, porosity has an effect on the surface-area-to-volume ratio. The relationship between the surface area, volume and porosity is the greatest at 50% porosity; as porosity increases, this relationship starts to decrease.[62] They offered an explanation as well, speculating that the inner surface overlaps more when the porosity of the scaffold is lower and less than that when it is higher.[62] The change of porosity affects the permeability of the scaffold. Under the same flow rate, permeability increases with an increase in porosity, and the conductivity of the biological effect is stronger.[63,64]

The TPMS scaffold exhibited better permeability than the mesh scaffold. Ma et al.[65] found that I-WP is more permeable in the longitudinal fluid flow direction than that of the grid-based scaffold. With 80% porosity, a gyroid structure has the highest permeability and is more permeable than the grid scaffold.[66] The gyroid is also 10 times more permeable than the grid scaffold.[67] The permeability of the gyroid unit is greater than that of the primitive and diamond units when the porosity is 55%.[66] Castro et al.[68] 3D printed diamond, gyroid and primitive scaffolds with different porosity sizes to assess the effects of these three TPMS structures on permeability. The gyroid scaffold was found to have the highest penetration rate and the diamond scaffold had the worst results in the test.[68] Using four porosity levels – 50%, 60%, 70% and 80% – and diamond, gyroid and primitive structures, Santos et al.[69] arrived at this conclusion. Twelve scaffolds were made from these scaffolds, and the permeability of each was determined using the laws of Darcy, Forchheimer and weak inertia. Of the three types of scaffolds, the gyroid type was the most permeable and the diamond type was the least permeable. At 50 and 60% porosity, the gyroid had a higher permeability than that of the primitive; however, at 70% porosity, the permeabilities were equivalent. The primitive has the highest permeability at 80% porosity.[69] The permeability of radially graded scaffolds increases with porosity,
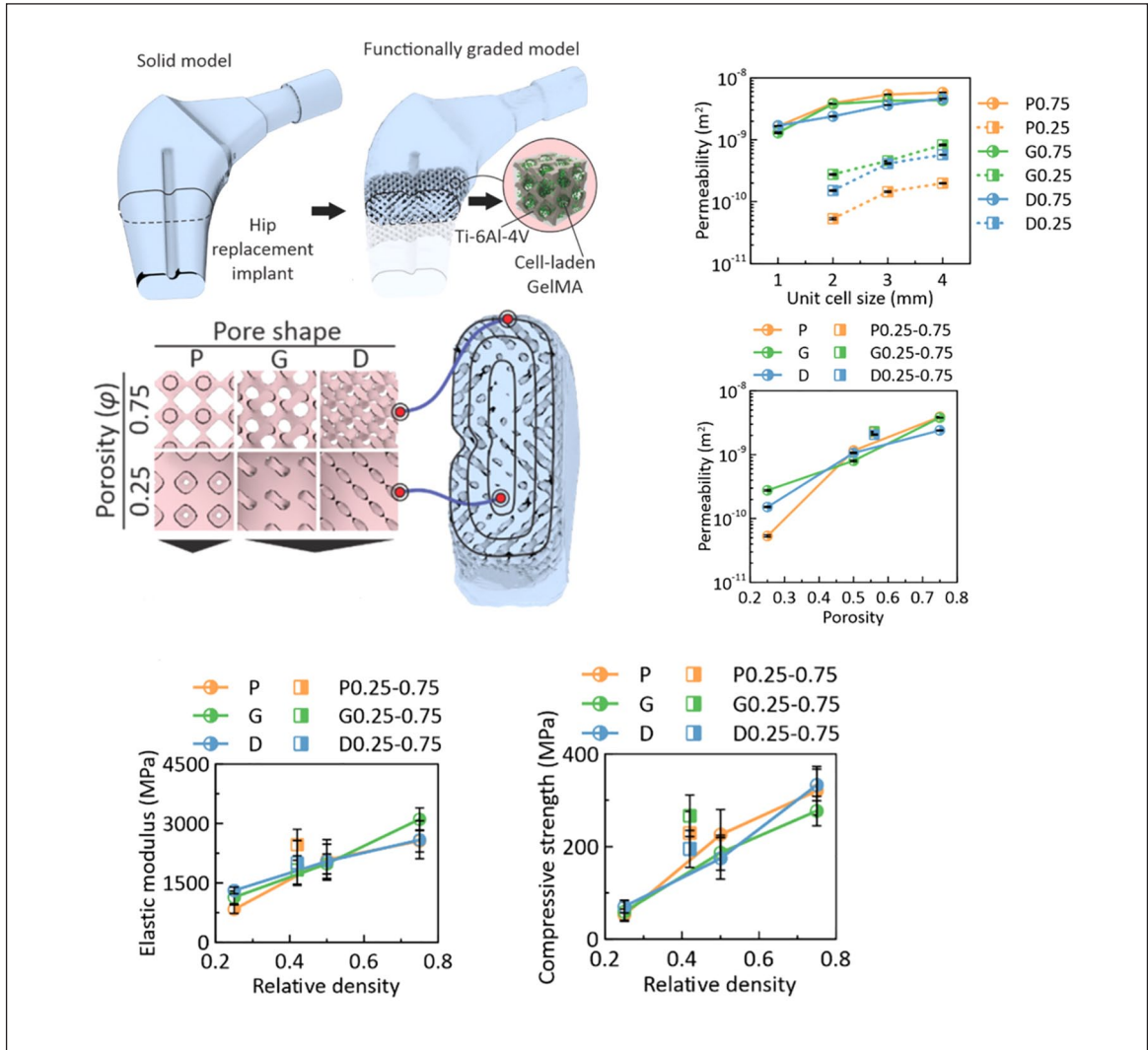
Figure 4. Outer hip was treated with a 75% porosity TPMS scaffold and the inner hip was treated with a 25% porosity TPMS scaffold. Reproduced from Alfieri et al.[40] with permission from Copyright 2023 The Authors.

surpassing that of uniform scaffolds.[10] In contrast, the structure of the femur (small porosity in the outer layer requires high strength, and the large porosity in the inner layer requires low strength) is the structure of the hip joint. The inherent structural characteristics of these two types of bone were explained by the experiments of Afshar et al.,[70] who indicated that the gradient structure with a radial increase from low to high relative density had higher strain energy absorption and strength compared to the gradient structure with a radial decrease from high to low relative density. The structure of the scaffold that Davoodi et al.[40] produced using the TPMS scaffold exhibits a progressive decrease in the porosity of the hip joint from the surface to the middle (Figure 4). With a larger porosity of 75%, the area closest to the surface of the scaffold has more permeability, which facilitates the infusion of cell-filled hydrogels. Owing to its architecture, which promotes inward bone growth and better bone integration, the scaffold cen-

tre has a lower porosity of 25%, thereby providing mechanical support to the implant.[40]

Young's modulus decreases as porosity increases in scaffolds, in accordance with the Gibson-Ashby model, which links porosity to mechanical qualities.[36] After analysing the mechanical characteristics of the 50% and 70% porosity gyroid scaffolds, Castro et al.[71] concluded that the Young's modulus of the 50% porosity scaffolds was more than double that of the 70% porosity scaffolds. A 3D printed PEEK scaffolds and polyether ketone/silicon nitride (PEEK/SiN) scaffolds with a gyroid structure and set porosity of 30%, 50% and 70% were produced by Du et al.[27] The findings of the compression experiment differ as a result of the different material composition; however, regardless of the type of scaffold printed, a 50% porosity scaffold has a compressive strength that is roughly three times greater than a 70% porosity scaffold.[27] The increase in the porosity of the scaffold and its deformation being
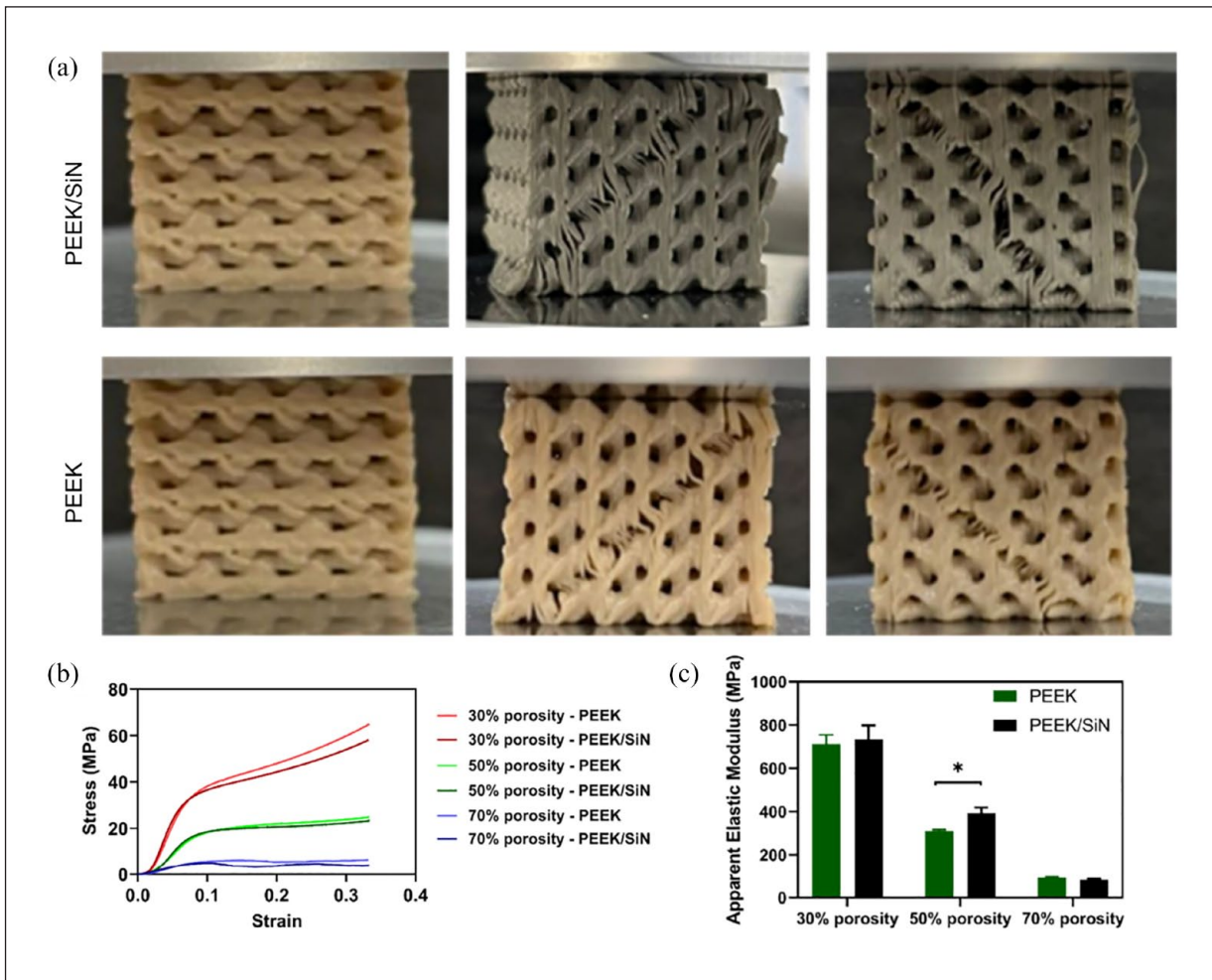
Figure 5. (a) Porosity of the scaffold from left to right is 30%, 50% and 70%, and the figure shows the state of the scaffold under pressure. (b) Stress–strain curves and (c) Apparent elastic modulus of PEEK and PEEK/SiN scaffolds with different porosities under vertical compression. Reproduced from Xiaoyu Du et al.[27] with permission from Copyright 2023 The Authors.

more severe is shown in Figure 5.[27] Within one to two days, the gyroid structure with 50% porosity exhibits strong cell adsorption.[28] Zhu et al.[72] prepared four kinds of gyroid scaffolds with porosity (40%, 50%, 60% and 70%) using β-TCP and implanted the stents into the mandibular defect of rabbits for four months. The results showed that the gyroid scaffold with 70% porosity showed excellent cell proliferation, adhesion and significantly enhanced osteogenesis and angiogenesis, which can effectively promote the bone regeneration of mandibular defects. The ratio of transverse strain to longitudinal strain in the direction of elastic load is known as Poisson's ratio.[73] Lu et al.[73] demonstrated that while the Poisson ratio of the F-RD and Schwarz P scaffolds declined, it increased for the gyroid, diamond and Fischer–Koch S scaffolds as their porosity increased. This indicates that the gyroid scaffold becomes more incompressible and the Schwarz P scaffold becomes more compressible with an increase in porosity.[73] The gradient porosity of the TPMS scaffold is more consistent with the physiological characteristics of bone and has stronger mechanical properties. Shi et al.[74] quantitatively examined the internal pore structure of the femoral head bone to ascertain the structural guidelines of various bone locations (Figure 6).

Lastly, 3D printing technology is essential to precisely create the required porosity structure.[74] Montazerian et al.[75] used FDM to print porous scaffolds made of polydimethylsiloxane (PDMS) with three distinct TPMS architectures to study how porosity affects fluid permeability and compression characteristics. The radial gradient porosity distribution scaffolds have a greater elastic modulus and fluid permeability than the uniform porosity scaffolds. Wang et al.[38] showed that the graded porous scaffold had a greater compressive toughness and elastic modulus, and that the high-porosity uniform porous scaffold's compression performance was comparable to that of the tibial spongy bone made of pork. Wang et al.[76] reached similar conclusions.
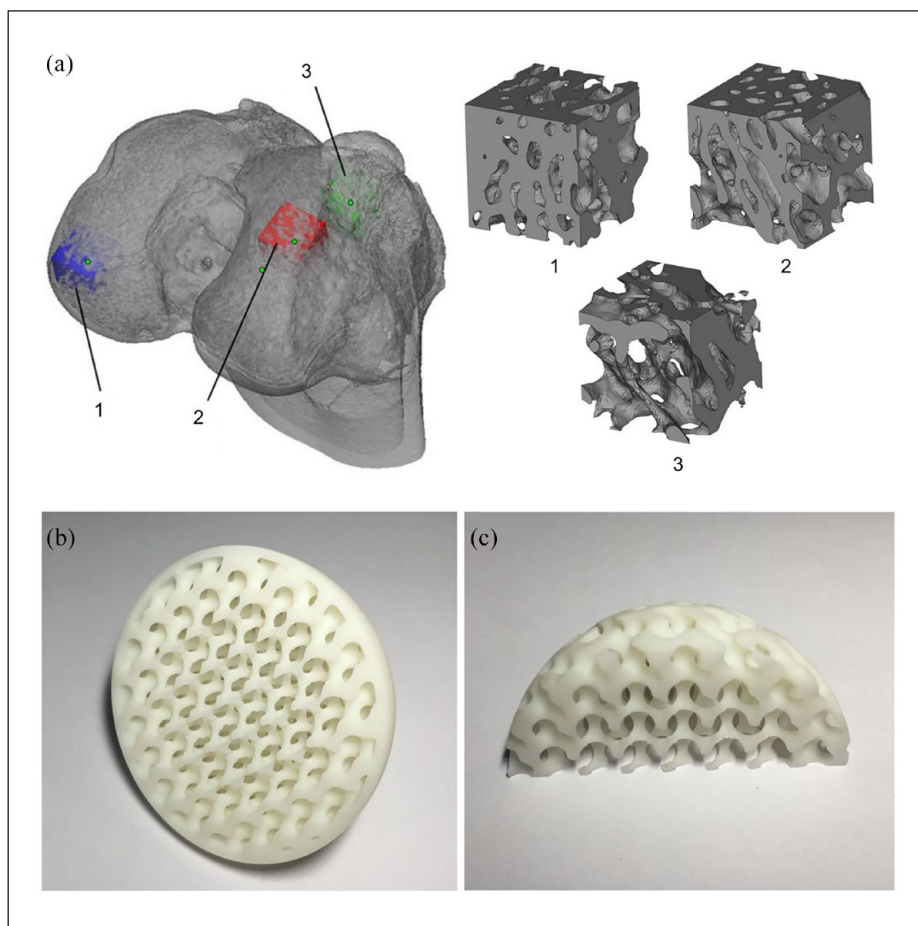
Figure 6. (a) Femoral condyle bone model: (1) femoral condyle bone top region, (2) femoral condyle bone lateral region, (3) femoral condyle bone internal region. (b, c) Printed bionic porous scaffold sample. Reproduced from Lu et al.[74] with permission from Copyright 2018 Science Edition.

Summary. The 50% porosity gyroid scaffold was the most suitable for mandibular regeneration, whereas the 70% porosity gyroid scaffold is more suitable for mandibular regeneration. The optimal porosity of other TPMS scaffolds requires further investigation. However, for human bone tissue, TPMS scaffolds with gradient porosities were more suitable than the TPMS scaffolds with uniform porosities and mesh scaffolds.

Surface curvature

Among all geometric rules considered, the collective effect of curvature on cell crowding was the main factor affecting the rate of cortical pore filling.[65] The mean curvature of the TPMS structure is zero, which is similar to the mean curvature of the trabecular bone indicated by others.[15] The product of major curvatures K1 (positive curvature, convex surface) and K2 (negative curvature, concave surface) yields the Gaussian curvature K of a surface point.[24] Every surface point of TPMS has a hyperbolic structure with a distinct Gaussian curvature.[24] TPMS is characterised by negative discrete Gaussian curvature, which is a unique feature of interconnected morphologies.[77] From a microscopic point of view, the cell migration behaviour and local tissue formation will be affected by the curvature when the local curvature of the scaffold surface is larger than the cell size range.[32,41] Low or high surface curvature will affect certain cell proliferation or differentiation; surfaces with a finer surface curvature distribution may promote homogenous tissue regeneration, whereas surfaces with more uneven curvature may promote cell differentiation.[65] Increased negative curvature areas encourage the growth of new cells because they allow cells to perceive surface curvature and differentiate within a certain range.[10,65] There are many different types of TPMS scaffolds, and although the TPMS of each structure have a high surface curvature, there are also high and low levels of cell growth promotion potential. When Lehder et al.[50] examined the rates of cell development of various TPMS structures, they discovered that the Split P and Lidinoid kinds offered the highest rates of cell proliferation (Figure 7). Ali investigated the effects of four distinct TPMS scaffold structures – double-diamond,
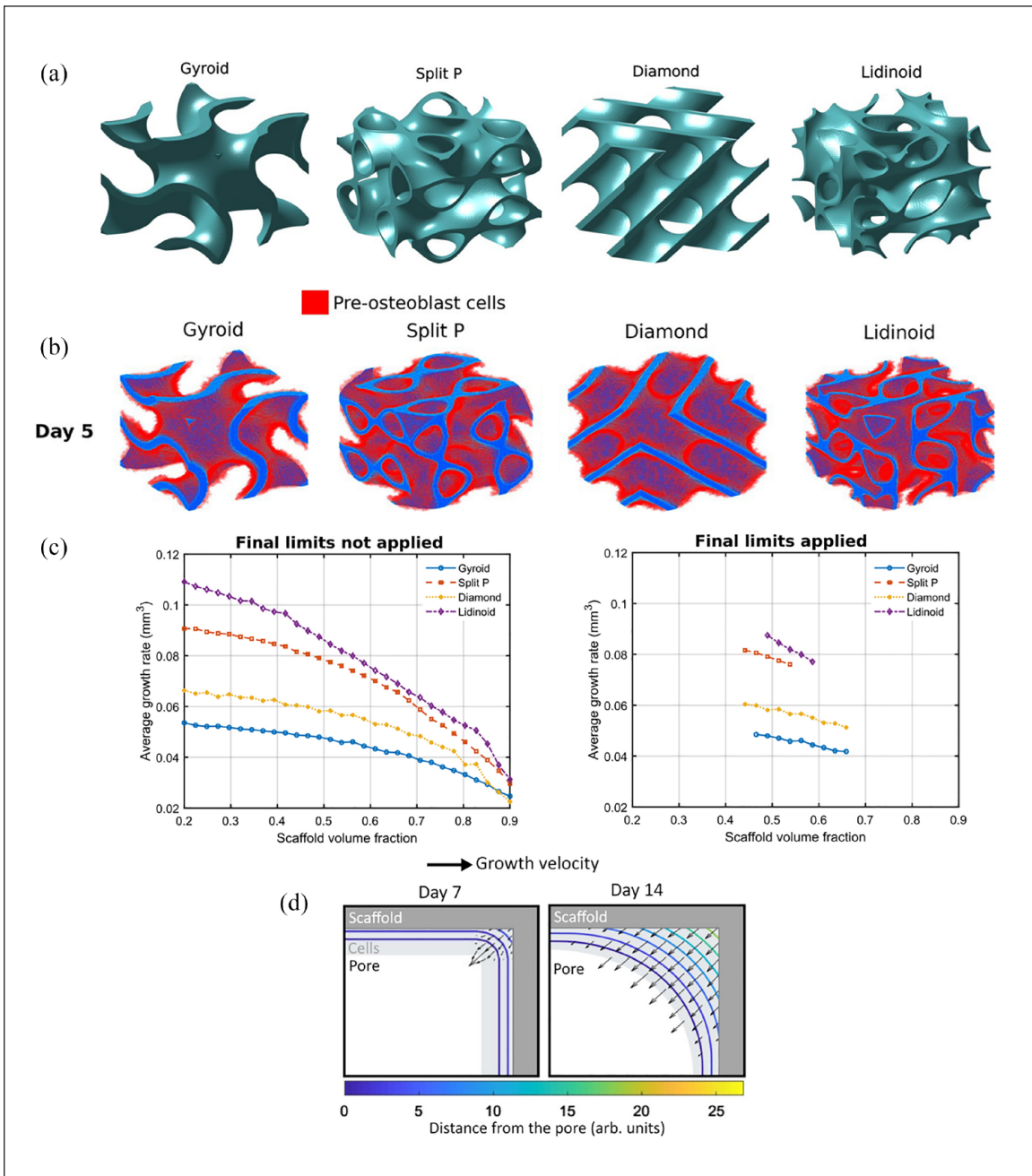
Figure 7. (a) Four different TPMS scaffolds. (b) Comparison of pre-osteoblasts after five days of growth on various TPMS scaffolds. (c) Average pre-osteoblast cell growth of each of the TPMS scaffold types after 21 culture days. (d) Principle of the cell growth model. Reproduced from Lehder et al.[50] with permission from Copyright 2021 Springer Nature.

gyroid, FR-D and primitive – with 80% porosity on cell adhesion.[60] Consequently, seven times as many cells were trapped by the double-diamond scaffold model as by the simpler scaffold.[60]

Blanquer et al.[32] created eight distinct kinds of poly(trimethylene carbonate) (PTMC) scaffolds with TPMS structures and the same porosity but varied curvatures using stereolithography. The curvature distribution influences both the uniformity of the element distribution

and the shear stress produced by the fluid inside the TPMS structure.[32] Li et al.[41] used AlSi10Mg powder to create scaffolds with various TPMS structures. Subsequently, they subjected the scaffolds to mechanical testing, which showed that the stretched TPMS structure, for a given porosity, has a more concentrated Gaussian curvature, higher elastic modulus and longer fatigue life. Altering the surface curvature could significantly enhance the overall mechanical properties of the TPMS devices. A

larger percentage of the local surface is near the cylinder, and therefore, the mechanical properties improve when the mean curvature approaches zero. The cylindrical surfaces experience less concentrated stress than the spherical and hyperboloidal surfaces when exposed to external forces.[41]

Summary. The average curvature of the TPMS structure is zero and characterised by a negative discrete Gaussian curvature, which affects the adhesion and mechanical properties of the cells. The microstructure of TPMS is closely related to its structural characteristics, which contributes to the structural characteristics of the TPMS scaffold.

Structural characteristics of TPMS scaffold

The capacity of a material to stimulate bone regeneration is closely correlated with its structural ability, which indicates that various materials may be employed to modify the strain distribution and promote inward bone growth. Changes in cell diffusion and strain distribution are caused by the structural properties of scaffolds, which modify the volume and distribution of regenerated bone.[78] Although the TPMS scaffolds promote bone regeneration because of their structural features, common scaffolds do so mostly because of advancements in technology and materials. The studies conducted by Liu et al.[34] demonstrate the significant effect that structure has on osteogenic differentiation. They used DLP to print hydroxyapatite (HA) ceramic scaffolds with three distinct structures: body-centred cubic (BCC), face-centred cubic (FCC) and TPMS (Figure 8).[34] In vitro research revealed that the expression levels of osteoblast proteins in rat BMSCs were TPMS, FCC and BCC, ranging from high to low, following 21 days of osteogenic induction on three scaffolds with distinct topologies. This was confirmed again by Myakinin et al.[37] The structural characteristics of the TPMS scaffold can make up for the shortcomings of the material. For example, calcium phosphate materials such as HA and tricalcium phosphate (TCP) are widely used because of their biocompatibility, high levels of bioactivity (bone conduction, bone inductance and bone integration) and similarity to the composition of human bone minerals; however, the biggest disadvantage of this material is that it is too brittle. Their brittleness can be partially mitigated by the structural properties of TPMS.[33] Baumer et al.[33] used a low-cost technique that combines robotic casting with layered photopolymerisation to successfully 3D print hydroxyapatite Fischer–Koch S scaffolds. With a porosity of 74.05%, which is within the optimal range for bone tissue creation. This TPMS scaffold provides structural qualities to compensate for the flaws of the material and lessens the brittleness of hydroxyapatite.[33]

Extremely high surface area to volume ratio

A higher surface-area-to-volume ratio indicates that the scaffold is more open to the environment, allowing it to engage in greater environmental interaction.[55] Numerous biological and cellular processes, including ion exchange, oxygen diffusion and nutrient transport, occur at the surface.[8] The porous structure of TPMS is modest in size but has a large surface area, which increases the possibility that bone cells may adhere to these structures.[8] Consequently, TPMS scaffolds with a greater surface-area-to-volume ratio can make cells more accurate biological cues.[11] The surface area of the cell is inversely correlated with its lattice size; that is, the larger the surface area offered in a given volume, the smaller is the cell utilised to occupy that space.[56] Kowalczyk et al.[77] developed the surface-constrained Metropolis Monte Carlo algorithm, which was used to study the graphitisation reaction process of diamond, gyroid and Schwarz P. The TPMS reaches a cubic lattice parameter of 8 nm. They were found to have a specific surface area of $\sim 2700\,m^2/g$ and are comparable to that of graphene. Meanwhile, infinite continuous surfaces with smooth seams provide improved mechanical qualities and less stress concentration.[11] Lu et al.[62] discovered that of the five TPMS (diamond, gyroid, Schwarz P, Fischer–Koch S and F-RD), the Fischer–Koch S scaffold had the highest surface area to volume ratio. F-RD, diamond, gyroid and Schwarz P scaffolds have next surface to volume ratios. A wide surface area is desirable for scaffolds used in bone tissue engineering to obtain greater bone integration. According to Belda et al.,[79] lamellar TPMS scaffolds with a low volume fraction are the most suitable.

Summary. A wide surface area is desirable for scaffolds used in bone tissue engineering to obtain greater bone integration. According to Belda et al., lamellar TPMS scaffolds with a low volume fraction are the most suitable.

Less stress concentration

The TPMS structure prevents localised concentrations of stress and provides a smooth stress distribution throughout its surrounding surface because of its continuously curved surface.[80] Similar to the axial compressive stress of a human load-bearing bone, a uniform static pressure of 100 MPa is applied to the support axially in the finite element model simulation. According to the finite element model research, traditional scaffolders feature a significant stress concentration, which is mostly concentrated at the junction between the structure and immediate strain region, according to finite element model research.[7] According to the modelling results, the maximum stress of the junction scaffold is greater than 400 MPa, which is greater than the damage value. Under the same load, the

Figure 8. (a) Single cell, scaffold and top view of BCC, FCC and TPMS. (b) 3D printed HA scaffold with BCC, FCC and TPMS structure and enlarged image. (c) Compressive strain–compressive stress and (d) compressive strength of HA scaffolds. (e) Detection of the cell growth of BMSCs cells at 1, 4 and 7 days using the CCK8 method. (f) Expression activity of ALP on DLP 3D printed HA scaffolds after BMSCs cells were cultured on scaffolds for 1, 4 and 7 days. Reproduced from He et al.[34] with permission from Copyright 2023 Royal Society of Chemistry .

maximum stress of the TPMS scaffold is only 150 MPa, the stress distribution is more uniform, its stress concentration is lower, and it falls entirely within the necessary range of compressive strength.[7] According to the modelling results, the maximum stress of the junction scaffold is greater than 400 MPa, which is greater than 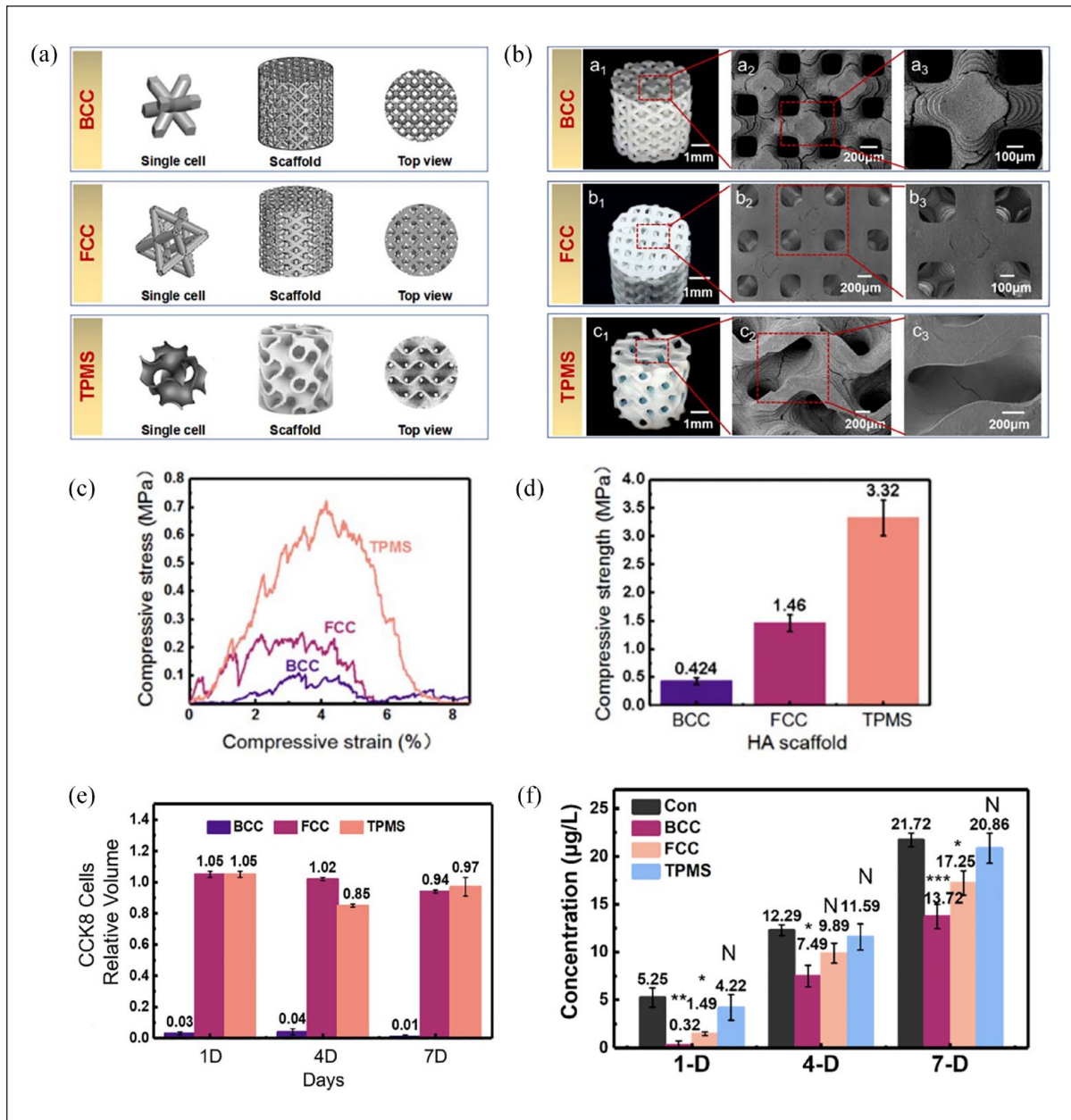the damage value. Under the same load, the maximum stress of the TPMS scaffold is only 150 MPa, the stress distribution is more uniform, its stress concentration is lower, and it falls

entirely within the necessary range of compressive strength.[17] The meniscus is a pair of crescent-shaped cartilages that sit between the tibia and two bearing articular surfaces of the femur. It performs crucial functions in the knee joint including auxiliary lubrication, load transfer and mechanical shock absorption. The TPMS scaffold can be placed in the meniscus because of its low stress concentration. The deformable primitive created by Li et al.[62] aids in effective load transfer by lowering the meniscus's

extrusion displacement, stress limit and stress concentration to preserve the articular cartilage.

Summary. Stress concentration is inevitable in all scaffolds and bone tissues. We can only reduce the stress concentration, but cannot eliminate it. TPMS scaffolds have lower stress concentrations than that of traditional mesh scaffolds. A radially graded TPMS can achieve a smooth transition, which makes the TPMS stent more advantageous.

Stronger mechanical properties

The human cancellous bone, proximal tibia, femoral neck and skull have elastic moduli ranging from 20–5000, 200–2800, 750–4500 and 2038.39–5990.36 MPa, respectively. The various bone tissues of the human body have varying yield strengths ranging from 0.56–240 MPa.[10] The Ti6Al4V scaffold with the TPMS structure manufactured by FDM was utilised by Zhang et al.[10] The yield strengths of the graded scaffold and the elastic model ranged from 45.9–262.3 and 1157.95–4566.7 MPa, respectively, which are within the range required by the elastic modulus of the human resinous bone. In addition, they satisfy requirements of the bone tissue. Zhang et al.[7] used SLA to fabricate HAp scaffolds with six TPMS structures (Split-P, diamond, Schwarz P, Dprime, lindinoid and gyroid). By evaluating the compressive strength of the HA scaffold, they discovered that the split-P scaffold could reach 150 MPa, whereas the conventional grid scaffold could only reach 12 MPa. Split-P scaffolds correspond to the compressive strength of cortical bone (100 MPa), whereas conventional mesh scaffolds equal the compressive strength of cancellous bone (2–12 MPa).[7] Scaffolds with split-P and conventional mesh were inserted into the 4 mm rabbit femur bone segmental defect. Four weeks later, the holes of the split-P scaffold showed more newly produced bone than those of the standard mesh scaffold.[7] Scaffolds with split-P and conventional mesh were inserted into the 4 mm rabbit femur bone segmental defect. Four weeks later, the holes of the split-P scaffold showed more newly produced bone than those of the standard mesh scaffold.[29] Alkaline phosphatase (ALP) staining revealed that the TPMS scaffold had a higher level of osteogenic differentiation capacity than that of the mesh-porous scaffold.[29] Liu used Bredigite to 3D print three different types of TPMS model scaffolds with porosities of 50%, 60% and 70%.[81] As a control experiment, an open-rod model with the same porosity was employed. The TPMS scaffolds with the same porosity exhibited greater ductility and compressive strength than the open-rod scaffolds. The difference is more noticeable with higher porosity.[81] These findings suggests that, in terms of compressive strength and osteogenic ability, TPMS scaffolds outperform conventional mesh scaffolds.

The mechanical characteristics of stretching-dominated constructions are higher because most materials are better at absorbing energy and suitable for axial mode loading.[70] For instance, Maskery et al.[82] discovered that primitive's relative elastic modulus was more than twice that of gyroid and diamond structures because it mostly displayed pillar stretching and buckling, whereas gyroid and diamond showed bending deformation. Another stretching-dominated structure with a large capacity absorption potential is the I-WP structure.[70] Li et al.[83] compared primitive, I-WP, diamond and gyroid structures and discovered that the I-WP structure is a better option when the support is subjected to axial force, whereas the primitive structure is more appropriate when the support is subjected to tangential force. When compared to diamond and gyroid scaffolds, Karimipour-Fard et al.[53] discovered that Neovius scaffolds showed inferior mechanical qualities. Barber et al.[57] reported that the gyroid scaffold has the highest compressive strength at 60°, whereas the diamond scaffold has the lowest at 45° and the highest at 0° and 90°. Sarabia-Vallejos printed gyroid and diamond supports using DLP, and the results showed that the former not only significantly enhanced the mechanical resistance of the material, but also had higher compressive strength than the latter.[84] In conclusion, the compressive strength of scaffolds-prepared with different structures under the same conditions is I-WP, primitive, gyroid, diamond, Neovius and traditional grid structure, in that order. However, the gyroid scaffold can match the requirements of human bone tissue although it has a low compressive strength. Kelly et al.[85] implanted the gyroid scaffold in rats with femoral cortical bone defects and discovered that the scaffold could heal segmental abnormalities at 12 weeks, with torsion stiffness reaching 54% and torsion strength reaching 38% of the intact femur. Wang et al.[86] proposed changing the lattice structure of the TPMS scaffold by self-torsion to adjust the mechanical properties. The Young's modulus of the support decreased with an increase in the torsion angle, which suggests that TPMS scaffolds can undergo self-torsion when used for bone defects to reduce the mechanical properties of scaffolds to adapt to the environment of the defect site.

Summary. The compressive strengths of the scaffolds were I-WP, primitive, gyroid, diamond, Neovius and traditional mesh structures, in that order, and all TPMS scaffolds exhibited stronger mechanical properties than those of the traditional mesh scaffolds. TPMS scaffolds can meet and even change the compressive strength (independently of the compressive strength of cancellous or cortical bone) by self-torsion to adapt to individual bone defects.

Better cell adhesion

The compressive strengths of the scaffolds were I-WP, primitive, gyroid, diamond, Neovius and traditional mesh structures, in that order, and all TPMS scaffolds exhibited stronger mechanical properties than those of the traditional

mesh scaffolds. TPMS scaffolds can meet and even change the compressive strength (independently of the compressive strength of cancellous or cortical bone) by self-torsion to adapt to individual bone defects.[65] BMSCs are non-hematopoietic stem cells that exist in bone marrow and have multidirectional differentiation potential.[87] The BMSCs can move from their niche into the peripheral circulation and pass through vessel walls to reach the bone defect area.[88] Macrophages, which are important innate immune effector cells, can effectively improve the cellular activity of BMSCs and have a low inflammatory response to scaffold materials, thereby promoting the proliferation and differentiation of BMSCs.[89] Studies have shown that TPMS scaffolds can promote the polarisation of macrophages toward M2 type and reduce the expression of pro-inflammatory genes, which allows BMSCs to attach to TPMS scaffolds more quickly.[89] Osteoblasts can be divided into three distinct stages of increasing differentiation: osteoprogenitor, preosteoblast and osteoblast.[90] Runt-related transcription factor 2 promotes the differentiation of BMSCs into proosteoblasts. During the maturation stage, WNT-β-catenin signalling acts on preosteoblasts, which defines the differentiation of the cell to an osteoblast.[90] Osteoclasts originate from the haematopoietic lineage and differentiate to mature osteoclasts through the interaction of the macrophage colony-stimulating factor (M-CSF) and the receptor activator of nuclear factor-κB ligand (RANKL).[90] At this point, the basic cells of reconstructed bone tissue are in place.

The ability of a fluid to move through a material or structure can be expressed quantitatively as permeability.[10] The inward expansion of tissues is mostly dependent on a mix of porosity, zigzagging, pore size and interconnectivity, which regulates the matrix volume available for cell attachment and vascularisation.[69] A highly porous structure encourages the creation of new tissues and achieves great cell inward growth.[91] The higher permeability significantly improves the wetting properties of the hydrophobic scaffold and increases the rate of cell sedimentation during static mesenchymal stem cell (MSC) inoculation.[49] The ability of the porous structure to convey flow to every part of the structure at a rate that permits the host cells to adhere to the surface is made possible by its permeability, which is utilised in bone regeneration.[8] TPMS scaffolds are constructed of continuous surface structures with optimised fluid permeability, and they exhibit open cell networks that provide continuous porosity for vascularisation and highly interconnected pores that provide sufficient space for cell attachment, promoting cell adhesion and retention.[92] Wall shear stress (WSS) generated by fluid flow within the scaffold is an important factor to consider because it affects cell distribution during new tissue formation. The WSS is caused by the relative motion between the wall of the support and fluid in the support. Pins et al.[93]

analysed the average WSS of the diamond and gyroid scaffolds using computational fluid dynamics (CFD) and found that different levels of WSS caused mesenchymal stromal cells to produce different mechanical signals, which in turn led to differences in cell differentiation processes. Pins et al.[93] analysed the average WSS of the diamond and gyroid scaffolds using computational fluid dynamics (CFD). The WSS level of the scaffold mesh with a smooth surface topology of tetrahedral elements is 35% higher than that of the equivalent scaffold with the non-smooth surface topology of hexahedral elements. Ye et al.[51] 3D printed a molten porous scaffold with a combination of primitive and gyroid TPMS structures to mimic real bone tissue using SLM technology (Figure 9). Utilising a Navier–Stokes model, CFD was employed to examine how the permeability of TPMS porous scaffolds was affected by the inner G unit's rotation angle and direction. They observed that the permeability of the 13 models ranged from 5.70015×10^{-8} to $6.33725 \times 10^{-8}\,m^2$, fulfilling the permeability requirements of human bone tissue. They adjusted the rotation angle of the G unit from 0° to 180° in 15° increments (Figure 9).[51] This suggests that the rotation angle of the TPMS unit affects permeability; however, it still satisfies bone tissue requirements and promotes cell adhesion.

The special structure of TPMS can promote the adhesion of cells required for osteogenesis. Both concave and convex TPMS structures can regulate the behaviour and function of bone marrow-derived stem cells during osteogenic differentiation and angiogenic paracrine signalling. The convex surface of the TPMS scaffold can promote the bone formation of MSCs because the cytoskeletal forces on the convex surface deform the nucleus and increase lamin A levels.[24] In addition, TPMS scaffold can accelerate the paracrine effect of MSCs, thereby promoting the angiogenesis of endothelial cells for accelerating the formation of new blood vessels, and thus, bone regeneration.[24] For the development of preosteoblasts on the scaffold surface, two significant findings exist: (a) The rate of bone tissue and cell proliferation increases with an increase in the concave curvature. (b) On flat and convex surfaces, very little bone tissue and cell proliferation are observed until the local environment becomes concave as a result of cell growth in other locations.[50] In addition, it is believed that tissue regeneration proceed more quickly on curved surfaces than that on flat surfaces.[56, 60] This indicates that the convex and convex surfaces of TPMS structures encourage tissue regeneration more successfully than the mesh planes. On the concave surface, osteoblasts have a better development direction.[94] The creation of bone tissue grew with the growth of the concave curvature of the scaffold structure; additionally, the concave region of the scaffold structure formed tissue preferentially and had a better effect on bone tissue regeneration than the convex
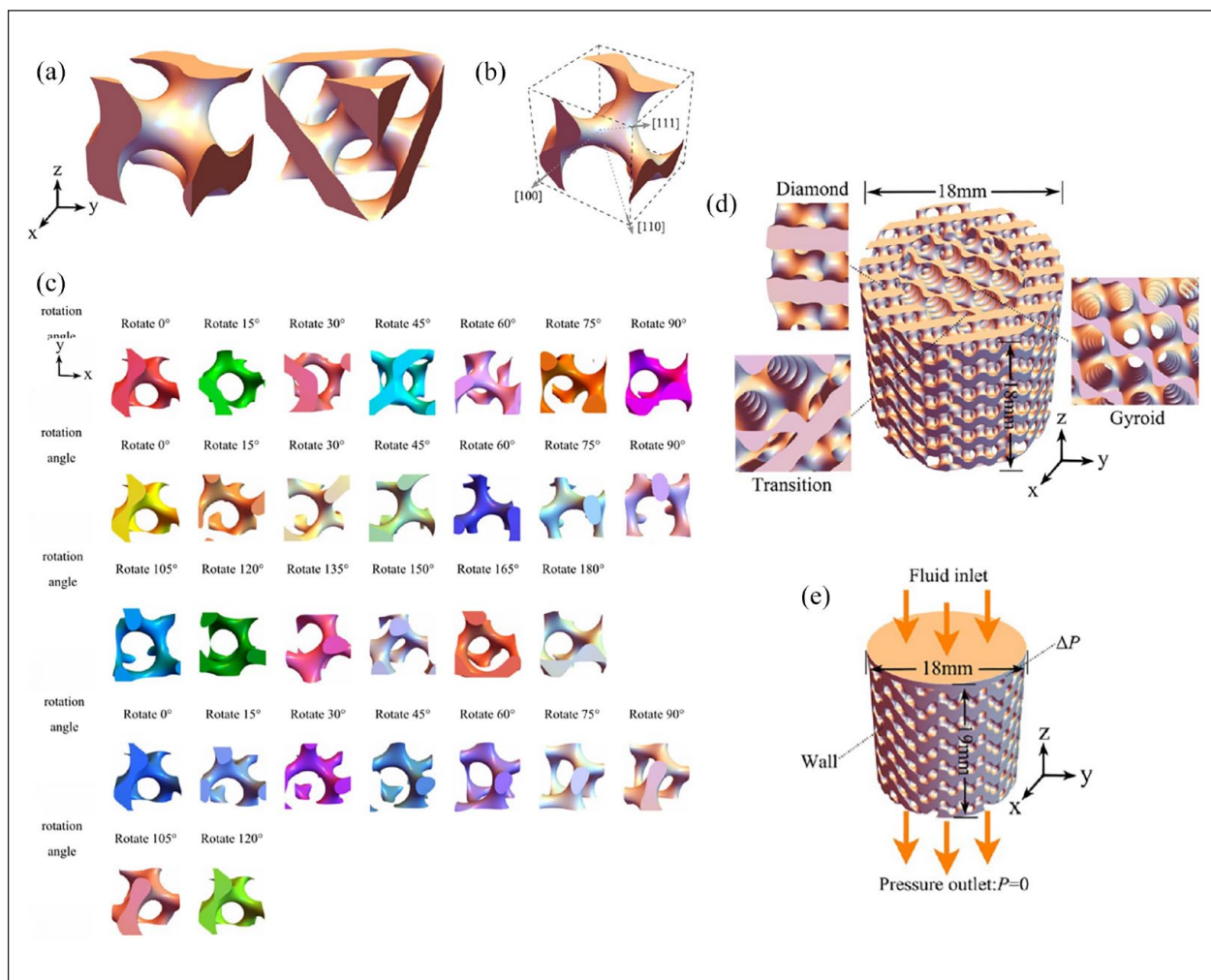
Figure 9. (a) G unit structure and D unit structures. (b) [100], [110] and [111] directions of the G unit structure. (c) G unit rotating at different angles. (d) Inner layer of the scaffold is gyroid and the outer layer is primitive. (e) Fluid simulation model and boundary conditions. Reproduced from Zeng et al.[51] with permission from Copyright 2023 American Chemical Society.

region.[41] In addition, osteoclasts for bone resorption are more advantageous in the concave surface.[94]

Summary. The concave surface of the TPMS structure is more suitable for the attachment of osteoclasts, preosteoblasts and osteoblasts, whereas the convex surface of the TPMS structure is more suitable for attaching the BMSC. In addition, the excellent fluid permeability of the TPMS scaffolds provides favourable conditions for bone regeneration.

Future and prospect

The following criteria should be fulfilled by scaffolds used in bone tissue engineering: Biocompatibility, surface characteristics and biodegradability are crucial elements of bone graft scaffolds, and therefore, it is important to (a) mimic the chemical composition and nanostructure of bone surface, (b) mimic the structural and cell interaction characteristics of bone extracellular matrix, (c) provide initial mechanical strength and stiffness sufficient to replace lost bone and support osteoblast proliferation and differentiation as well as the expression of bone ECM and (d) have a 3D porous interconnect network sufficiently strong for vascular tissue to grow inward.[95] The TPMS scaffold satisfies all aforementioned requirements because of its structural features.

The TPMS scaffolds have been investigated extensively in various medical fields. For example, TPMS scaffolds have great potential for application in oral implantology, and their high mechanical strength indicates that they can be used instead of dental implants. Titanium alloys, which are used to make conventional dental implants, have a substantially larger Young's modulus than the surrounding bone tissue.[96] A significant mismatch in the Young's modulus between the implant and surrounding bone occurs when a load is applied to the implant, leading to an uneven

distribution of stress at the interface between the implant and bone, creating a stress shielding effect that can cause the surrounding bone tissue to atrophy.[96] This raises the possibility of inflammation around the implant. The surrounding bone tissue is in an active reconstruction state, which encourages the formation of bone tissue when the stress on the bone tissue is between 20 and 60 MPa. Within the range of 60–120 MPa, the surrounding bone tissue experiences microdamage that eventually surpasses its capacity for self-healing. This results in damage to bone tissue, which can lead to pathological alterations. The widespread consensus is that the fracture strength of bone tissue, also known as the bone bearing capacity, is limited to 120 MPa.[96] The TPMS scaffolds with varying porosities were created by Song et al.[96] using 3D-printing technology, and they discovered that both primitive and gyroid scaffolds with a porosity of less than 40% could withstand the maximum stress in the adjacent 20–60 MPa range. Accordingly, TPMS scaffolds may be a more suitable substitute for dental implants compared to conventional titanium implants. Moreover, TPMS may encourage the formation of new bone tissue surrounding the implant, thereby leading to stable, long-term bone integration. A few researchers used TPMS in breast reconstruction, and it is evident that breast and bone tissue are two entirely different structures. The breast needs to be highly resilient, has a low tissue-like elastic modulus, high structural stability and a high load buffer capacity, while the bone tissue needs to be hard. Using FDM technology, Zhu et al.[97] created a TPMS scaffold with several parallel channels that allowed the elastic modulus to be adjusted as required. They infused a polyethylene glycol diacrylate/gelatin methacrylate hydrogel containing human adipose stem cells into the scaffold by perfusion and UV curing to enhance the environment for cell proliferation. In addition, the resulting scaffold's elastic modulus was 0.2–0.83 MPa, while the native breast tissue had an elastic modulus of 0.002–1 MPa.[97] This support's potential to rebound can reach 80% of its initial height. Scholars also prepared the radial grading scaffold with an I-WP structure, which is an aperture spanning from 500 μm in the centre to 800 μm at the periphery and serving as the orbital contents. This scaffold exhibited moderate mechanical strength, complete vascularisation and outstanding antibacterial activity against *Staphylococcus aureus* and *Escherichia coli*. Further, it offers an excellent procedure for enhancing ocular reconstruction.[98] The use of TPMS scaffolds in conjunction with antibacterial medications is essential for bone tissue engineering. Garcia et al.[23] incorporated an extract of Bacillus roseum in the gyroid scaffold to enhance bone regeneration and demonstrate antibacterial activities against both S. aureus and *Streptococcus mutans*. Moreno et al.[99] combined propolis extract wollastone particles with the gyroid scaffold and discovered that this combination had antibacterial activity against osteomyelitis-causing S. aureus and *Staphylococcus epidermidis*, and it did not alter the mechanical, thermal or physical properties of the scaffold, which are important findings for oral and maxillofacial surgeons. Treatment options for the osteomyelitis of the jaw have expanded.

The unique structure of the TPMS scaffold confers several benefits, including enhanced permeability that facilitates cell adhesion, migration and proliferation; high mechanical strength; a porous structure that imitates the properties of natural bone; and the ability to prevent stress shielding. Research demonstrated that Fischer–Koch S scaffolds are better suited because of their almost isotropic elastic characteristics because the cortical bone is an isotropic tissue. Scaffolds with strong anisotropic properties (such as gyroids) are more suited for the anisotropic mechanical behaviour of cancellous bone.[73] Similar to this, primitive and I-WP surface structures are ideally suited to replace injured cortical bone, whereas diamond and gyroid surface structures offer superior cell adsorption and proliferation qualities, making them a viable option for replacing trabecular bone.[17]

Limitations

The TPMS scaffold is not perfect, and it has some limitations, as listed below:

1. The preparation method is single and can only be prepared by 3D printing.
2. Some errors were observed between the designed and printed scaffolds. For example, small-aperture plugging and support surface roughness can be increased. This is because the preparation process has not yet reached the ideal requirements, which requires us to continuously improve the technology and overcome the process limits of 3D printing.[72,76,100–102]
3. It is difficult to reverse design an anisotropic TPMS scaffold based on the mechanical properties of the bone defect site, which requires further effort to achieve truly personalised bone defects.[103]
4. The largest limitation is that TPMS scaffolds are still in preclinical research; experiments are also in cell and animal experiments, and there is still a long way to go before they can be truly applied in humans.

We believe that research on TPMS scaffolds in tissue engineering has just begun and TPMS scaffolds have great prospects for personalised bone defects in the future.

Abbreviations

AdMSC	Adipose-derived mesenchymal stromal cell
ALP	Alkaline phosphatase

AM	Additive manufacturing
BCC	Body-centred cubic
BMSC	Bone marrow mesenchymal stem cell
CFD	Computational fluid dynamics
D	Diamond
DLP	Digital light processing
ECM	Extracellular matrix
FCC	Face-centred cubic
FDM	Fused deposition modelling
FE:	Finite element
G	Gyroid
GO	Graphene oxide
HA	Hydtoxyapatite
hMSC	Human mesenchymal stem cell
M-	CSF Macrophage colony-stimulating factor
P	Primitive
PDMS	Polydimethylsiloxane
PEEK/SiN	Polyether ketone/silicon nitride
PLA	Polylatic acid
PTMC	Poly(trimethylene carbonate)
RANKL	Receptor activator of nuclear factor-κB ligand
rMSCs	Rat mesenchymal stem cells
SLA	Stereolithography
SLM	Selective Laser Melting
TCP	Tricalcium phosphate
TPMS:	Triply periodic minimal surfaces
WSS	Wall shear stress
3D	Three dimension
β-TCP	β-tricalcium phosphate

Author Contributions

J.M.: Initial concept, data collection and analysis, initial draft and editing of the article. Y.L.: Data collection and analysis, initial draft and editing of the article. Y.M. participated in data collection and analysis. Q.G. participated in data collection. P.Z. participated in data collection. B.M. participated in the data collection. J.W. (Jue Wang): participated in data collection. J.W. (Jing Wang): helped draft the manuscript, reviewed and edited the article. Y.F. helped draft, reviewed and edited the manuscript. All the authors have read and agreed to the published version of the manuscript.

Availability of data and material

The datasets used and analysed in the current study are available from the corresponding author upon reasonable request.

Declaration of conflicting interests

The author(s) declared no potential conflicts of interest with respect to the research, authorship, and/or publication of this article.

Funding

ORCID iD

Jiaqi Ma https://orcid.org/0009-0006-4482-1355

References

1. Liu Y, Sun X, Yu J, et al. Platelet-rich fibrin as a bone graft material in oral and maxillofacial bone regeneration: classification and summary for better application. *Biomed Res Int* 2019; 2019: 3295756.
2. Zhang P, Qi J, Zhang R, et al. Recent advances in composite hydrogels: synthesis, classification, and application in the treatment of bone defects. *Biomater Sci* 2024; 12: 308–329.
3. Nauth A, Schemitsch E, Norris B, et al. Critical-size bone defects: is there a consensus for diagnosis and treatment? *J Orthop Trauma* 2018; 32 Suppl 1: S7–S11.
4. Moussa NT and Dym H. Maxillofacial bone grafting materials. *Dent Clin North Am* 2020; 64: 473–490.
5. Wickramasinghe ML, Dias GJ and Premadasa K. A novel classification of bone graft materials. *J Biomed Mater Res B Appl Biomater* 2022; 110: 1724–1749.
6. Zhao Z, Li J, Wei Y, et al. Design and properties of graded polyamide12/hydroxyapatite scaffolds based on primitive lattices using selective laser sintering. *J Mech Behav Biomed Mater* 2022; 126: 105052.
7. Zhang Q, Ma L, Ji X, et al. High-strength hydroxyapatite scaffolds with minimal surface macrostruc tures for load-bearing bone regeneration. *Adv Funct Mater* 2022; 32: 2204182.
8. Karaman D and Ghahramanzadeh Asl H. The effects of sheet and network solid structures of similar TPMS scaffold architectures on permeability, wall shear stress, and velocity: a CFD analysis. *Med Eng Phys* 2023; 118: 104024.
9. Liu F, Ran Q, Zhao M, et al. Additively manufactured continuous cell-size gradient porous scaffolds: pore characteristics, mechanical properties and biological responses in vitro. *Materials* 2020; 13: 2589.
10. Zhang J, Chen X, Sun Y, et al. Design of a biomimetic graded TPMS scaffold with quantitatively adjust able pore size. *MaterDes* 2022; 218: 110665.
11. Vijayavenkataraman S, Zhang L, Zhang S, et al. Triply periodic minimal surfaces sheet scaffolds for tissue engineering applications: an optimization approach toward biomimetic scaffold design. *ACS Appl Bio Mater* 2018; 1: 259–269.
12. Maevskaia E, Guerrero J, Ghayor C, et al. Triply periodic minimal surface-based scaffolds for bone tissue engineering: a mechanical, in vitro and in vivo study. *Tissue Eng Part A* 2023; 29: 507–517.
13. Shen M, Li Y, Lu F, et al. Bioceramic scaffolds with triply periodic minimal surface architectures guide early-stage bone regeneration. *Bioact Mater* 2023; 25: 374–386.
14. Li L, Shi J, Zhang K, et al. Early osteointegration evaluation of porous Ti6Al4V scaffolds designed based on triply periodic minimal surface models. *J Orthop Translat* 2019; 19: 94–105.
15. Zhou X, Jin Y and Du J. Functionally graded scaffolds with programmable pore size distribution based on triply periodic minimal surface fabricated by selective laser melting. *Materials* 2020; 13: 5046.

16. Yoo DJ. Porous scaffold design using the distance field and triply periodic minimal surface models. _Biomaterials_ 2011; 32: 7741–7754.

17. Elenskaya N, Tashkinov M, Vindokurov I, et al. Understanding of trabecular-cortical transition zone: Numerical and experimental assessment of multi-morphology scaffolds. _J Mech Behav Biomed Mater_ 2023; 147: 106146.

18. Mustafa NS, Akhmal NH, Izman S, et al. Application of computational method in designing a unit cell of bone tissue engineering scaffold: a review. _Polymers_ 2021; 13: 1584.

19. Colella R, Chietera FP and Catarinucci L. Analysis of FDM and DLP 3D-printing technologies to prototype electromagnetic devices for RFID applications. _Sensors_ 2021; 21: 897.

20. Yuan L, Ding S and Wen C. Additive manufacturing technology for porous metal implant applications and triple minimal surface structures: a review. _Bioact Mater_ 2019; 4: 56–70.

21. Pugliese R and Graziosi S. Biomimetic scaffolds using triply periodic minimal surface-based porous structures for biomedical applications. _SLAS Technol_ 2023; 28: 165–182.

22. Bandyopadhyay A, Mitra I and Bose S. 3D printing for bone regeneration. _Curr Osteoporos Rep_ 2020; 18: 505–514.

23. Garcia C, Orozco Y, Betancur A, et al. Fabrication of polycaprolactone/calcium phosphates hybrid scaffolds impregnated with plant extracts using 3D printing for potential bone regeneration. _Heliyon_ 2023; 9: e13176.

24. Yang Y, Xu T, Bei HP, et al. Gaussian curvature-driven direction of cell fate toward osteogenesis with triply periodic minimal surface scaffolds. _Proc Natl Acad Sci USA_ 2022; 119: e2206684119.

25. Pagac M, Hajnys J, Ma QP, et al. A review of vat photopolymerization technology: materials, applications, challenges, and future trends of 3D printing. _Polymers_ 2021; 13: 598.

26. Bouakaz I, Drouet C, Grossin D, et al. Hydroxyapatite 3D-printed scaffolds with Gyroid-Triply periodic minimal surface porous structure: fabrication and an in vivo pilot study in sheep. _Acta Biomater_ 2023; 170: 580–595.

27. Du X, Ronayne S, Lee SS, et al. 3D-printed PEEK/silicon nitride scaffolds with a triply periodic minimal surface structure for spinal fusion implants. _ACS Appl Bio Mater_ 2023; 6: 3319–3329.

28. Diez-Escudero A, Harlin H, Isaksson P, et al. Porous polylactic acid scaffolds for bone regeneration: a study of additively manufactured triply periodic minimal surfaces and their osteogenic potential. _J Tissue Eng_ 2020; 11: 2041731420956541.

29. Guo W, Yang Y, Liu C, et al. 3D printed TPMS structural PLA/GO scaffold: Process parameter optimization, porous structure, mechanical and biological properties. _J Mech Behav Biomed Mater_ 2023; 142: 105848.

30. Chen B, Sun X, Liu D, et al. A novel method combining VAT photopolymerization and casting for the fabrication of biodegradable Zn-1Mg scaffolds with triply periodic minimal surface. _J Mech Behav Biomed Mater_ 2023; 141: 105763.

31. Afshar M, Anaraki AP, Montazerian H, et al. Additive manufacturing and mechanical characterization of graded porosity scaffolds designed based on triply periodic minimal surface architectures. _J Mech Behav Biomed Mater_ 2016; 62: 481–494.

32. Blanquer SBG, Werner M, Hannula M, et al. Surface curvature in triply-periodic minimal surface architectures as a distinct design parameter in preparing advanced tissue engineering scaffolds. _Biofabrication_ 2017; 9: 025001.

33. Baumer V, Gunn E, Riegle V, et al. Robocasting of ceramic fischer-koch s scaffolds for bone tissue engineering. _J Funct Biomater_ 2023; 14: 251.

34. Liu K, Zhou Q, Zhang X, et al. Morphologies, mechanical and in vitro behaviors of DLP-based 3D printed HA scaffolds with different structural configurations. _RSC Adv_ 2023; 13: 20830–20838.

35. Lv J, Jin W, Liu W, et al. Selective laser melting fabrication of porous Ti6Al4V scaffolds with triply periodic minimal surface architectures: structural features, cytocompatibility, and osteogenesis. _Front Bioeng Biotechnol_ 2022; 10: 899531.

36. Naghavi SA, Tamaddon M, Marghoub A, et al. Mechanical characterisation and numerical modelling of TPMS-based gyroid and diamond Ti6Al4V scaffolds for bone implants: An integrated approach for translational consideration. _Bioengineering_ 2022; 9: 504.

37. Myakinin A, Turlybekuly A, Pogrebnjak A, et al. In vitro evaluation of electrochemically bioactivated Ti6Al4V 3D porous scaffolds. _Mater Sci Eng C Mater Biol Appl_ 2021; 121: 111870.

38. Wang Z, Liao B, Liu Y, et al. Influence of structural parameters of 3D-printed triply periodic minimal surface gyroid porous scaffolds on compression performance, cell response, and bone regeneration. _J Biomed Mater Res B Appl Biomater_ 2024; 112: e35337.

39. Lv Y, Liu G, Wang B, et al. Pore Strategy design of a Novel NiTi-Nb biomedical porous scaffold based on a triply periodic minimal surface. _Front Bioeng Biotechnol_ 2022; 10: 910475.

40. Davoodi E, Montazerian H, Esmaeilizadeh R, et al. Additively manufactured gradient porous Ti-6Al-4V hip replacement implants embedded with cell-laden gelatin methacryloyl hydrogels. _ACS Appl Mater Interfaces_ 2021; 13: 22110–22123.

41. Li Z, Chen Z, Chen X, et al. Mechanical properties of triply periodic minimal surface (TPMS) scaffolds: considering the influence of spatial angle and surface curvature. _Biomech Model Mechanobiol_ 2023; 22: 541–560.

42. Zhang H, Zhang M, Zhai D, et al. Polyhedron-like biomaterials for innervated and vascularized bone regeneration. _Adv Mater_ 2023; 35: e2302716.

43. Maevskaia E, Khera N, Ghayor C, et al. Three-dimensional printed hydroxyapatite bone substitutes designed by a novel periodic minimal surface algorithm are highly osteoconductive. _3D Print Addit Manuf_ 2023; 10: 905–916.

44. Barba A, Maazouz Y, Diez-Escudero A, et al. Osteogenesis by foamed and 3D-printed nanostructured calcium phosphate

scaffolds: effect of pore architecture. *Acta Biomater* 2018; 79: 135–147.

45. Ye X, Zhang Y, Liu T, et al. Beta-tricalcium phosphate enhanced mechanical and biological properties of 3D-printed polyhydroxyalkanoates scaffold for bone tissue engineering. *Int J Biol Macromol* 2022; 209: 1553–1561.

46. Buenzli PR, Lanaro M, Wong CS, et al. Cell proliferation and migration explain pore bridging dynamics in 3D printed scaffolds of different pore size. *Acta Biomater* 2020; 114: 285–295.

47. Kapfer SC, Hyde ST, Mecke K, et al. Minimal surface scaffold designs for tissue engineering. *Biomaterials* 2011; 32: 6875–6882.

48. Blanquer SBG and Grijpma DW. Triply periodic minimal surfaces (TPMS) for the generation of porous architectures using stereolithography. *Methods Mol Biol* 2021; 2147: 19–30.

49. Al-Ketan O and Abu Al-Rub RK. Multifunctional mechanical metamaterials based on triply periodic minimal surface lattices. *Adv Eng Mater* 2019; 21: 1900524.

50. Lehder EF, Ashcroft IA, Wildman RD, et al. A multiscale optimisation method for bone growth scaffolds based on triply periodic minimal surfaces. *Biomech Model Mechanobiol* 2021; 20: 2085–2096.

51. Ye J, He W, Wei T, et al. Mechanical properties directionality and permeability of fused triply periodic minimal surface porous scaffolds fabricated by selective laser melting. *ACS Biomater Sci Eng* 2023; 9: 5084–5096.

52. Jaber M, Poh PSP, Duda GN, et al. PCL strut-like scaffolds appear superior to gyroid in terms of bone regeneration within a long bone large defect: An in silico study. *Front Bioeng Biotechnol* 2022; 10: 995266.

53. Karimipour-Fard P, Behravesh AH, Jones-Taggart H, et al. Effects of design, porosity and biodegradation on mechanical and morphological properties of additive-manufactured triply periodic minimal surface scaffolds. *J Mech Behav Biomed Mater* 2020; 112: 104064.

54. Rajagopalan S and Robb RA. Schwarz meets Schwann: design and fabrication of biomorphic and duratraxic tissue engineering scaffolds. *Med Image Anal* 2006; 10: 693–712.

55. Jin Y, Kong H, Zhou X, et al. Design and characterization of sheet-based gyroid porous structures with bioinspired functional gradients. *Materials* 2020; 13: 3844.

56. Al-Ketan O, Lee DW, Rowshan R, et al. Functionally graded and multi-morphology sheet TPMS lattices: design, manufacturing, and mechanical properties. *J Mech Behav Biomed Mater* 2020; 102: 103520.

57. Barber H, Kelly CN, Nelson K, et al. Compressive anisotropy of sheet and strut based porous Ti-6Al-4V scaffolds. *J Mech Behav Biomed Mater* 2021; 115: 104243.

58. Günther F, Wagner M, Pilz S, et al. Design procedure for triply periodic minimal surface based biomimetic scaffolds. *J Mech Behav Biomed Mater* 2022; 126: 104871.

59. Chung JJ, Yoo J, Sum BST, et al. 3D printed porous methacrylate/silica hybrid scaffold for bone substitution. *Adv Healthc Mater* 2021; 10: e2100117.

60. Ali D. Effect of scaffold architecture on cell seeding efficiency: a discrete phase model CFD analysis. *Comput Biol Med* 2019; 109: 62–69.

61. Qu M, Wang C, Zhou X, et al. Multi-dimensional printing for bone tissue engineering. *Adv Healthc Mater* 2021; 10: e2001986.

62. Lu Y, Cheng L, Yang Z, et al. Relationship between the morphological, mechanical and permeability properties of porous bone scaffolds and the underlying microstructure. *PLoS ONE* 2020; 15: e0238471.

63. Asbai-Ghoudan R, Ruiz de, Galarreta S and Rodriguez-Florez N. Analytical model for the prediction of permeability of triply periodic minimal surfaces. *J Mech Behav Biomed Mater* 2021; 124: 104804.

64. Zhang Y, Sun N, Zhu M, et al. The contribution of pore size and porosity of 3D printed porous titanium scaffolds to osteogenesis. *Biomater Adv* 2022; 133: 112651.

65. Ma S, Song K, Lan J, et al. Biological and mechanical property analysis for designed heterogeneous porous scaffolds based on the refined TPMS. *J Mech Behav Biomed Mater* 2020; 107: 103727.

66. Li Z, Chen Z, Chen X, et al. Effect of surface curvature on the mechanical and mass-transport properties of additively manufactured tissue scaffolds with minimal surfaces. *ACS Biomater Sci Eng* 2022; 8: 1623–1643.

67. Flores-Jimenez MS and Fuentes-Aguilar RQ. Bone tissue scaffolds designed with a porosity gradient based on triply periodic minimal surfaces using a parametric approach. *Annu Int Conf IEEE Eng Med Biol Soc* 2021; 2021: 1209–1212.

68. Castro APG, Pires T, Santos JE, et al. Permeability versus design in TPMS scaffolds. *Materials* 2019; 12: 1313.

69. Santos J, Pires T, Gouveia BP, et al. On the permeability of TPMS scaffolds. *J Mech Behav Biomed Mater* 2020; 110: 103932.

70. Afshar M, Pourkamali Anaraki A and Montazerian H. Compressive characteristics of radially graded porosity scaffolds architectured with minimal surfaces. *Mater Sci Eng C Mater Biol Appl* 2018; 92: 254–267.

71. Castro APG, Ruben RB, Gonçalves SB, et al. Numerical and experimental evaluation of TPMS Gyroid scaffolds for bone tissue engineering. *Comput Methods Biomech Biomed Engin* 2019; 22: 567–573.

72. Zhu H, Wang J, Wang S, et al. Additively manufactured bioceramic scaffolds based on triply periodic minimal surfaces for bone regeneration. *J Tissue Eng* 2024; 15: 1-15.

73. Lu Y, Zhao W, Cui Z, et al. The anisotropic elastic behavior of the widely-used triply-periodic minimal surface based scaffolds. *J Mech Behav Biomed Mater* 2019; 99: 56–65.

74. Shi J, Zhu L, Li L, et al. A TPMS-based method for modeling porous scaffolds for bionic bone tissue engineering. *Sci Rep* 2018; 8: 7395.

75. Montazerian H, Mohamed MGA, Montazeri MM, et al. Permeability and mechanical properties of gradient porous PDMS scaffolds fabricated by 3D-printed sacrificial templates designed with minimal surfaces. *Acta Biomater* 2019; 96: 149–160.

76. Wang Y, Chen S, Liang H, et al. Design and fabrication of biomimicking radially graded scaffolds via digital light processing 3D printing for bone regeneration. *J Mater Chem B* 2023; 11: 9961–9974.

77. Kowalczyk P, Furmaniak S, Neimark AV, et al. Surface-constrained metropolis monte carlo: simulation of reactions on triply periodic minimal surfaces. *J Phys Chem A* 2024; 128: 1725–1735.

78. Asbai-Ghoudan R, Nasello G, Pérez M, et al. In silico assessment of the bone regeneration potential of complex porous scaffolds. *Comput Biol Med* 2023; 165: 107381.

79. Belda R, Megías R, Marco M, et al. Numerical analysis of the influence of triply periodic minimal surface structures morphometry on the mechanical response. *Comput Methods Programs Biomed* 2023; 230: 107342.

80. Guo X, Zheng X, Yang Y, et al. Mechanical behavior of TPMS-based scaffolds: a comparison between minimal surfaces and their lattice structures. *SN Appl Sci* 2019; 1: 1145.

81. Liu D, Zhou X, Wang F, et al. Research and analysis of the properties of bredigite-based 3D-printed bone scaffolds. *Int J Bioprint* 2023; 9: 708.

82. Prause M, Schulz HJ and Wagler D. Rechnergestützte Führung von Fermentationsprozessen, Teil 2. *Acta Biotechnologica* 1984; 4: 143–151.

83. Li Z, Chen Z, Chen X, et al. Effect of unit configurations and parameters on the properties of Ti-6Al-4V unit-stacked scaffolds: A trade-off between mechanical and permeable performance. *J Mech Behav Biomed Mater* 2021; 116: 104332.

84. Sarabia-Vallejos MA, De la Fuente SR, Tapia P, et al. Development of biocompatible digital light processing resins for additive manufacturing using visible light-induced RAFT polymerization. *Polymers* 2024; 16: 472.

85. Kelly CN, Lin AS, Leguineche KE, et al. Functional repair of critically sized femoral defects treated with bioinspired titanium gyroid-sheet scaffolds. *J Mech Behav Biomed Mater* 2021; 116: 104380.

86. Wang Z, Xu M, Du J, et al. Experimental and numerical investigation of polymer-based 3D-printed lattice structures with largely tunable mechanical properties based on triply periodic minimal surface. *Polymers* 2024; 16: 711.

87. Lin Z, He H, Wang M, et al. MicroRNA-130a controls bone marrow mesenchymal stem cell differentiation towards the osteoblastic and adipogenic fate. *Cell Prolif* 2019; 52: e12688.

88. Fu X, Liu G, Halim A, et al. Mesenchymal stem cell migration and tissue repair. *Cells* 2019; 8: 784.

89. Jiang C, Ding M, Zhang J, et al. 3D printed porous zirconia biomaterials based on triply periodic minimal surfaces promote osseointegration in vitro by regulating osteo-immunomodulation and osteo/angiogenesis. *ACS Appl Mater Interfaces* 2024; 16: 14548–14560.

90. Salhotra A, Shah HN, Levi B, et al. Mechanisms of bone development and repair. *Nat Rev Mol Cell Biol* 2020; 21: 696–711.

91. Davoodi E, Montazerian H, Zhianmanesh M, et al. Template-enabled biofabrication of thick 3D tissues with patterned perfusable macrochannels. *Adv Healthc Mater* 2022; 11: e2102123.

92. Gabrieli R, Wenger R, Mazza M, et al. Design, stereolithographic 3D printing, and characterization of TPMS scaffolds. *Materials* 2024; 17: 654.

93. Pires THV, Dunlop JWC, Castro APG, et al. Wall shear stress analysis and optimization in tissue engineering TPMS scaffolds. *Materials* 2022; 15: 7375.

94. Yuste I, Luciano FC, González-Burgos E, et al. Mimicking bone microenvironment: 2D and 3D in vitro models of human osteoblasts. *Pharmacol Res* 2021; 169: 105626.

95. Liu Y, Luo D and Wang T. Hierarchical structures of bone and bioinspired bone tissue engineering. *Small* 2016; 12: 4611–4632.

96. Song K, Wang Z, Lan J, et al. Porous structure design and mechanical behavior analysis based on TPMS for customized root analogue implant. *J Mech Behav Biomed Mater* 2021; 115: 104222.

97. Zhu X, Chen F, Cao H, et al. Design and fused deposition modeling of triply periodic minimal surface scaffolds with channels and hydrogel for breast reconstruction. *Int J Bioprint* 2023; 9: 685.

98. Wang J, Peng Y, Chen M, et al. Next-generation finely controlled graded porous antibacterial bioceramics for high-efficiency vascularization in orbital reconstruction. *Bioact Mater* 2022; 16: 334–345.

99. Moreno AI, Orozco Y, Ocampo S, et al. Effects of propolis impregnation on polylactic acid (PLA) scaffolds loaded with wollastonite particles against staphylococcus aureus, staphylococcus epidermidis, and their coculture for potential medical devices. *Polymers* 2023; 15: 2629.

100. Naghavi SA, Wang H, Varma SN, et al. On the morphological deviation in additive manufacturing of porous Ti6Al4V scaffold: a design consideration. *Materials* 2022; 15: 4729.

101. Lu Y, Huo Y, Zou J, et al. Comparison of the design maps of TPMS based bone scaffolds using a computational modeling framework simultaneously considering various conditions. *Proc Inst Mech Eng H Med* 2022; 236: 1157–1168.

102. Lu Y, Cui Z, Cheng L, et al. Quantifying the discrepancies in the geometric and mechanical properties of the theoretically designed and additively manufactured scaffolds. *J Mech Behav Biomed Mater* 2020; 112: 104080.

103. Liu W, Zhang Y, Lyu Y, et al. Inverse design of anisotropic bone scaffold based on machine learning and regenerative genetic algorithm. *Front Bioeng Biotechnol* 2023; 11: 1241151.